



**HAL**  
open science

# Earliest life on Earth: Evidence from the Barberton Greenstone Belt, South Africa

Martin Homann

► **To cite this version:**

Martin Homann. Earliest life on Earth: Evidence from the Barberton Greenstone Belt, South Africa. Earth-Science Reviews, 2019, 196, 10.1016/j.earscirev.2019.102888 . hal-02933520

**HAL Id: hal-02933520**

**<https://hal.univ-brest.fr/hal-02933520>**

Submitted on 8 Sep 2020

**HAL** is a multi-disciplinary open access archive for the deposit and dissemination of scientific research documents, whether they are published or not. The documents may come from teaching and research institutions in France or abroad, or from public or private research centers.

L'archive ouverte pluridisciplinaire **HAL**, est destinée au dépôt et à la diffusion de documents scientifiques de niveau recherche, publiés ou non, émanant des établissements d'enseignement et de recherche français ou étrangers, des laboratoires publics ou privés.

# 1 Earliest life on Earth: Evidence from the Barberton Greenstone Belt, South Africa

2  
3  
4  
5  
6  
7  
8  
9  
10  
11  
12  
13  
14  
15  
16  
17  
18  
19  
20  
21  
22  
23  
24  
25  
26  
27  
28  
29  
30  
31  
32  
33  
34  
35  
36  
37  
38  
39  
40  
41  
42  
43  
44  
45  
46  
47  
48  
49  
50  
51  
52  
53  
54  
55  
56

10 Martin Homann<sup>1</sup>

11 <sup>1</sup>European Institute for Marine Studies, CNRS-UMR6538 Laboratoire Géosciences Océan, Technopôle  
12 Brest-Iroise, 29280 Plouzané, France. \*corresponding author: martin.homann@univ-brest.fr

13  
14  
15  
16  
17  
18  
19  
20  
21  
22  
23  
24  
25  
26  
27  
28  
29  
30  
31  
32  
33  
34  
35  
36  
37  
38  
39  
40  
41  
42  
43  
44  
45  
46  
47  
48  
49  
50  
51  
52  
53  
54  
55  
56

9 Studies investigating the structure and diversity of Earth's record of life older than 3.2 Ga are  
10 restricted to two locations worldwide in which sedimentary rocks have escaped regional high-grade  
11 metamorphism and penetrative deformation: the Pilbara Craton of Western Australia and the Barberton  
12 Greenstone Belt (BGB) in the Kaapvaal Craton of South Africa. This paper provides a South African  
13 perspective on the evidence of Paleoproterozoic life; a record that is often overlooked in the literature. It aims  
14 to summarize and critically review previously reported claims of early life in the BGB, gives an overview  
15 of the latest findings, and provides an outlook on potential future discoveries.

16  
17  
18  
19  
20  
21  
22  
23  
24  
25  
26  
27  
28  
29  
30  
31  
32  
33  
34  
35  
36  
37  
38  
39  
40  
41  
42  
43  
44  
45  
46  
47  
48  
49  
50  
51  
52  
53  
54  
55  
56

16 The ~15 km thick, volcanic-sedimentary succession making up the Barberton Supergroup was  
17 deposited between 3.55 to ca. 3.20 Ga and can be subdivided in three stratigraphic units that provide a  
18 unique window into a diverse and widespread Paleoproterozoic microbial ecosystem landscape. Putative  
19 biosignatures occur almost throughout the entire BGB stratigraphy and range from carbonaceous cherts  
20 containing filamentous, spheroidal, and lenticular microstructures, traces of hydrothermal biofilms,  
21 photosynthetic microbial mats, remnants of pseudocolumnar stromatolites, and large, organic-walled  
22 spheroidal microfossils of currently unknown affinity. The BGB also contains one of the world's oldest  
23 known record of tufted microbial mats, which extensively colonized tidally-influenced, siliciclastic  
24 shorelines and were most likely formed by filamentous photosynthesizers. Other mat-associated  
25 biosignatures include silicified gas bubbles, domes and lenses that likely formed due to metabolic activity  
26 or the decay of buried organic matter. Some of these subsurface voids beneath the cohesive mats were  
27 inhabited by the earliest known forms of cavity-dwelling microbial communities that were probably  
28 dominated by chemotrophic or photosynthetic microbes. Recently discovered terrestrial microbial mats,  
29 once thriving in a fluvial-dominated setting, represent the oldest macroscopically-visible fossil traces of life  
30 on land, which is also supported by the occurrence of nearby paleosols that carry signals of biogenic sulfur  
31 fractionation.

32  
33  
34  
35

32 The wealth of preserved microbial biosignatures from marine, fluvial, hydrothermal, and possibly  
33 planktonic settings combined with the high spatial and temporal resolution of the Barberton Greenstone  
34 Belt deposits is truly exceptional, consequently the BGB deserves an equal level of attention and protection  
35 for future generations like its Australian counterpart.

57  
58  
59  
60  
61  
62  
63  
64  
65  
66  
67  
68  
69  
70  
71  
72  
73  
74  
75  
76  
77  
78  
79  
80  
81  
82  
83  
84  
85  
86  
87  
88  
89  
90  
91  
92  
93  
94  
95  
96  
97  
98  
99  
100  
101  
102  
103  
104  
105  
106  
107  
108  
109  
110  
111  
112

36  
37  
38  
39  
40  
41  
42  
43  
44  
45  
46  
47  
48  
49  
50  
51  
52  
53  
54  
55  
56  
57  
58  
59  
60  
61  
62  
63  
64  
65  
66  
67  
68  
69

## 1. Introduction

The Archean rock record is sparse, largely metamorphosed, and preserved in fragmented Greenstone Belts, which occur wedged in between plutonic and metamorphic rocks in the cratonic lithosphere of nearly all continents. However, only the Barberton Greenstone Belt (BGB) of South Africa and Swaziland and the contemporaneous Pilbara Greenstone Belts (PGBs) of Western Australia contain well-preserved sedimentary rocks of Paleoproterozoic age ( $>3.2$  Ga), which experienced only greenschist facies metamorphism and relatively minor deformation. With an area of  $\sim 6000$  km<sup>2</sup> and an age of  $\sim 3.55$ – $3.20$  Ga the BGB is significantly smaller and captures a slightly shorter time interval in comparison to the PGBs ( $\sim 60000$  km<sup>2</sup>,  $\sim 3.52$ – $2.94$  Ga), however, the deposits preserved in the BGB are characterized by often laterally consistent outcrops with correlatable facies, a generally better exposure, and very good accessibility. Lithified aquatic sediments in both of these volcano-sedimentary “enclaves” are considered the most suitable archive of ancient microbial life, as water is one of the fundamental requirements for life. Consequently, the sedimentary deposits have been extensively studied for traces of early life in these two localities and the reported findings have been critically reviewed especially for the Pilbara Greenstone Belts, where stromatolites, microfossils, and isotopic signals belong to the most dominant biosignatures (e.g. Allwood et al., 2006; Brasier et al., 2006; Wacey, 2009, 2012). The focus of this study here is to summarize and review the South African evidence of Paleoproterozoic life reported from the BGB, place them in a consistent stratigraphic framework, and discuss and evaluate the most recent findings.

## 2. Geology of the BGB

The Barberton Greenstone Belt of South Africa and Swaziland is located at the eastern margin of the Kaapvaal Craton and contains volcanic, shallow intrusive, and sedimentary rocks, ranging in age from  $<3.547$  to  $>3.219$  Ga (Byerly et al., 2019; Fig. 1). These age constraints are mainly derived from high-precision zircon U-Pb age dating of interbedded volcanic units and plutons surrounding the BGB, as well as detrital zircon geochronology. Rocks of the Barberton Supergroup (formerly named Swaziland Supergroup), are subdivided from base to top into three lithostratigraphic units: (1) the  $\sim 8$ – $10$  km thick, volcanic-dominated Onverwacht Group, which comprises the Komati, Hooggenoeg, Kromberg, and Mendon Formations (Viljoen and Viljoen, 1969; Anhaeusser, 1976; Lowe and Byerly, 2007; De Wit and Furnes, H., 2011); (2) the up to  $\sim 2$  km thick Fig Tree Group, predominantly composed of interlayered volcanoclastic strata that mark the final stages of major volcanism and the transition to deposition of terrigenous clastic units (Heinrichs and Reimer, 1977; Lowe, 1999a; Hofmann, 2005; Byerly et al., 2019); and (3) the up to  $3.5$  km thick, coarse-grained siliciclastic to conglomeritic Moodies Group, mainly derived

113  
114  
115  
116  
117  
118  
119  
120  
121  
122  
123  
124  
125  
126  
127  
128  
129  
130  
131  
132  
133  
134  
135  
136  
137  
138  
139  
140  
141  
142  
143  
144  
145  
146  
147  
148  
149  
150  
151  
152  
153  
154  
155  
156  
157  
158  
159  
160  
161  
162  
163  
164  
165  
166  
167  
168

70 from the erosion of underlying units and uplifted plutonic rocks (Eriksson, 1977; Heubeck and Lowe,  
71 1994a, 1994b, 1999). The dominant large-scale orogeny of the BGB occurred contemporaneously with  
72 deposition of the Moodies Group at 3.225–3.215 Ga (Lamb and Paris, 1988; Heubeck et al., 2013).  
73 Although the BGB strata experienced several phases of major deformation during which they were folded,  
74 faulted and altered, the rocks are generally well-preserved in locally very thick and laterally-traceable  
75 sections (De Ronde and De Wit, 1994; Toulkeridis et al., 1998; Lowe and Byerly, 1999). A major fault  
76 system, the Inyoka Fault, transects the BGB approximately medially and divides it into a northern and  
77 southern facies, characterized by distinct differences in the preserved stratigraphy and depositional facies  
78 of especially the Onverwacht and Fig Tree Groups (Fig. 2). Although approximately coeval, these deposits  
79 represent previously geographically separated successions that are now in tectonic contact with another  
80 (Byerly et al., 2019). The greenstone belt fill can be further subdivided into several tectonostratigraphic  
81 blocks, each bordered by numerous, steeply dipping large and small faults (Lowe, 1999a; Lowe et al.,  
82 2012). Most rocks in the central part of the BGB experienced alteration temperatures of >300°C (Xie et  
83 al., 1997; Toulkeridis et al., 1998; Tice et al., 2004), however some primary mineralogy, textures, and  
84 sedimentary structures have been preserved in many units due to the combination of early silicification and  
85 the local partitioning of strain (Byerly et al., 2019).

86  
87

### 88 **3. History of early life studies in the BGB**

89 The BGB has a long history of studies focusing on traces of early life and the reconstruction of its habitat,  
90 metabolism, biogeochemical cycling, and mode of preservation (Table 1). Since the mid-1960s the  
91 occurrence of lenticular, spheroidal, and filamentous microstructures, interpreted as possible cellular  
92 microfossils, has been reported from carbonaceous cherts of the Onverwacht Group\* (Barghoorn and  
93 Schopf, 1966; Pflug, 1966, 1967; Schopf and Barghoorn, 1967; Pflug et al., 1969; Barghoorn, 1971). \*[Note  
94 that these samples were collected from the same outcrop, which was originally assigned to the Fig Tree  
95 Group, but later revised and changed to the upper Onverwacht Group (Pflug, 1967; Schopf, 1975; Lowe  
96 and Knauth, 1977).] In the following years simple spherical and filamentous microstructures have also  
97 been described from other Onverwacht Group cherts of the Mendon and Kromberg Formation (Engel et al.,  
98 1968; Nagy and Nagy, 1969; Brooks and Shaw, 1971; Brooks et al., 1973; Muir and Hall, 1974; Muir and  
99 Grant, 1976; Knoll and Barghoorn, 1977), however the exact stratigraphic position was often not clearly  
100 indicated, which made it challenging to put the individual findings in context to each other. In fact, the  
101 insufficient knowledge of the BGB stratigraphy at that time and the often poorly studied depositional facies,  
102 and paleoenvironmental context of the analyzed samples are central problems of most of these pioneering  
103 studies. Due to their often simply morphology and wide size range the biogenicity of almost all of the early-

169  
170  
171  
172  
173  
174  
175  
176  
177  
178  
179  
180  
181  
182  
183  
184  
185  
186  
187  
188  
189  
190  
191  
192  
193  
194  
195  
196  
197  
198  
199  
200  
201  
202  
203  
204  
205  
206  
207  
208  
209  
210  
211  
212  
213  
214  
215  
216  
217  
218  
219  
220  
221  
222  
223  
224

104 reported microfossils has been questioned in several reviews (Schopf, 1975; Schopf and Walter, 1983;  
105 Altermann, 2001; Wacey, 2009), which suggested that except for the structures described by Muir and  
106 Grant (1976) and Knoll and Barghoorn (1977) all other findings should be treated as nonfossil artefacts,  
107 aggregates of amorphous carbonaceous matter or modern contaminants. More detailed sedimentological,  
108 geochronological, and tectonostratigraphic investigations of the BGB deposits (Lowe and Knauth, 1977;  
109 Kröner et al., 1991; Lowe and Byerly, 1999; Lowe et al., 2012), organic carbon isotope analysis (e.g. Oehler  
110 et al., 1972), the identification of possible stromatolites (de Wit et al., 1982; Byerly et al., 1986; Byerly and  
111 Palmer, 1991; Walsh, 2004), and new discoveries of mat-like laminations, lenticular, spheroidal, and  
112 filamentous microfossil in cherts of the Hooggenoeg, Kromberg, and Mendon Formations (Walsh and  
113 Lowe, 1985, 1999; Walsh, 1992; Westall et al., 2001; Glikson et al., 2008) supported previous findings  
114 (e.g. Pflug, 1966; Knoll and Barghoorn, 1977) and stimulated further investigations. In the following,  
115 carbonaceous laminations preserved in the shallow-water facies of the Buck Reef Chert (Kromberg  
116 Formation) have been studied in great detail and were interpreted as the remains of photosynthetic microbial  
117 mats (Tice and Lowe, 2004, 2006a, 2006b; Tice, 2009; Tice et al., 2011). Westall et al. (2006, 2011, 2015,  
118 2018) identified microbial biofilms and possible fossil bacteria in the Josefsdal Chert (Kromberg  
119 Formation) and suggested that these microbial communities were once thriving in a nearshore hydrothermal  
120 setting. Tubular, titanite-mineralized microstructures in basaltic pillow lava rims of the Hooggenoeg and  
121 Kromberg Formations were interpreted as being the result of microbial etching, and thus indicating the  
122 presence of submarine thermophilic microbial communities during basalt formation (Furnes, 2004;  
123 Banerjee et al., 2007; Furnes et al., 2007; Fliegel et al., 2010). However, the syngenicity and biogenicity of  
124 these putative oldest trace fossils has been strongly questioned and is currently still under debate  
125 (McLoughlin et al., 2012; Grosch and McLoughlin, 2014; Staudigel et al., 2015; Wacey et al., 2017;  
126 Hickman-Lewis et al., 2019 for a short review). More recently, the biogenicity of lenticular microfossils  
127 from the Kromberg Formation was further supported by *in situ* carbon isotope analysis (Oehler et al., 2017),  
128 while new findings of cell-like objects from the Buck Reef Chert were interpreted as degraded colonies of  
129 coccoidal bacteria (Kremer and Kaźmierczak, 2017). Moreover, Hickman-Lewis et al. (2018) reported  
130 carbonaceous laminations, resembling microbial biofilms and mats from the Middle Marker at the base of  
131 the Hooggenoeg Formation, making it to the most ancient claim for life in the BGB.  
132 In the last decade also the sand- and siltstones of Moodies Group (uppermost unit of the BGB), were  
133 carefully investigated for traces of early microbial life, which resulted in the discovery of large spheroidal  
134 microfossils (Javaux et al., 2010), widespread shallow-marine tufted microbial mats once formed by  
135 photosynthetic microorganisms (Noffke et al., 2006; Heubeck, 2009; Gamper et al., 2012; Homann et al.,  
136 2015) and remnants of cavity-dwelling microbial communities (Homann et al., 2016). Terrestrial microbial  
137 mats interbedded with fluvial sandstones and conglomerates, record a significant difference in their organic

225  
226  
227  
228  
229  
230  
231  
232  
233  
234  
235  
236  
237  
238  
239  
240  
241  
242  
243  
244  
245  
246  
247  
248  
249  
250  
251  
252  
253  
254  
255  
256  
257  
258  
259  
260  
261  
262  
263  
264  
265  
266  
267  
268  
269  
270  
271  
272  
273  
274  
275  
276  
277  
278  
279  
280

138 carbon and nitrogen isotopes in comparison with the tidal marine mats and represent the oldest  
139 macroscopically-visible trace of life on land (Homann et al., 2018). The presence of a Paleoproterozoic  
140 terrestrial biosphere is further supported by the Moodies Group paleosols that carry signals of biogenic  
141 sulfur fractionation (Nabhan et al., 2016a, 2016b). In the following, a selection of the most promising and  
142 best documented claims for early life from the Onverwacht and Moodies Groups of the BGB will be  
143 described and discussed in more detail.

144

#### 145 **4. The 3.55–3.26 Onverwacht Group**

146 The Onverwacht Group consists of a up to 10 km thick succession of mostly of mafic and ultramafic  
147 volcanic rocks with minor felsic volcanic flow units and tuffs (Lowe and Byerly, 1999). Subordinate  
148 sedimentary units formed during episodic breaks in eruptive activity and have been widely silicified to  
149 bedded cherts, which host a large number of the reported traces of early life in the BGB, including microbial  
150 mats, microfossils, and possible stromatolites. Moreover, rare asteroid ejecta layers, composed of impact  
151 spherules, fine ash and dust, locally occur as discrete beds and record distal impact events of large asteroids  
152 with diameters ranging between 20–50 km (Fig. 2; Lowe and Byerly, 1986, 2018). The Onverwacht Group  
153 comprises four different formations (Komati, Hooggenoeg, Kromberg, and Mendon), which each can be  
154 further subdivided into informal members (e.g. H1 - H6). Within each member the cherts, which are capping  
155 individual volcanic units are designated with a "c" (e.g. H4c; Lowe and Byerly, 1999; Byerly et al., 2019).  
156 Overlying the basal Komati Formation, the 3.472 - 3.416 Ga Hooggenoeg Formation consists of thick  
157 sequence of tholeiitic basalts, minor komatiites, and thin chert units and can reach a thickness of up to 3900  
158 m on the western limb of the Onverwacht Anticline (Viljoen and Viljoen, 1969b, Lowe and Byerly, 1999).  
159 The 3.416 – 3.334 Ga Kromberg Formation on the west limb of the Onverwacht Anticline comprises an up  
160 to 1800-m-thick succession of black and banded chert (Buck Reef Chert, K1), mafic lapilli tuff and  
161 lapillistone (K2), and tholeiitic basalt (K3), while on the eastern limb of the anticline massive pillow basalt  
162 is more abundant. The top of the formation is marked by a regionally traceable chert unit, the Footbridge  
163 Chert (K3c; Viljoen and Viljoen, 1969, Lowe and Byerly, 1999). Conformably overlying the Kromberg  
164 Formation, the 3.334 – 3.258 Ga Mendon Formation has a thickness of >600m and records an alternation of  
165 volcanic cycles, each characterized by a komatiitic flow unit capped by a chert layer (Byerly, 1999).

166

#### 167 **4.1 Microbial mats**

168 The first systematic stratigraphic and petrographic analysis of all carbonaceous cherts in the Hooggenoeg,  
169 Kromberg, and Mendon Formation of the Onverwacht Group was made by Walsh (1992) and Walsh and  
170 Lowe (1999), who distinguished three main types: black-and-white banded, massive black, and black  
171 laminated chert. The carbonaceous matter in these cherts occurs mostly in the form of: fine laminations (1

281  
282  
283  
284  
285  
286  
287  
288  
289  
290  
291  
292  
293  
294  
295  
296  
297  
298  
299  
300  
301  
302  
303  
304  
305  
306  
307  
308  
309  
310  
311  
312  
313  
314  
315  
316  
317  
318  
319  
320  
321  
322  
323  
324  
325  
326  
327  
328  
329  
330  
331  
332  
333  
334  
335  
336

172 – 20  $\mu\text{m}$  thick), carbonaceous wisps (10–50  $\mu\text{m}$  thick, 50–1000  $\mu\text{m}$  long) that are likely eroded fragments  
173 of the fine laminations, subrounded composite grains (100–1000  $\mu\text{m}$ ), and irregular-shaped simple grains  
174 (5–750  $\mu\text{m}$ ), and. Based on bulk  $\delta^{13}\text{C}_{\text{org}}$  values ranging between  $-40.8\text{‰}$  and  $-16.9\text{‰}$ , with a mean of  
175  $-29.8\text{‰}$  ( $n = 50$ ), Walsh and Lowe (1999) concluded that all the carbonaceous matter in the cherts is  
176 probably of biological origin, which was further supported by a detailed study of van Zuilen et al. (2007),  
177 combining Raman spectroscopy and SIMS (secondary ion mass spectrometry) analysis.  
178 In detail, the fine carbonaceous laminations that form layers of 0.5–2 cm thickness and occur predominantly  
179 in black-and-white banded cherts the Hooggenoeg (H2, H4c, H5c), Kromberg (K1, K3c), and Mendon  
180 Formation (M1c, M2c), were interpreted as remains of microbial mats (Walsh, 1992; Walsh and Lowe,  
181 1999; Trower and Lowe, 2016). The alternation of carbonaceous black bands with thin layers of pure  
182 (white) quartz in these cherts is likely comparable with alternating organic-rich and organic-poor sediments  
183 in modern microbial mats. The mats presumably formed in periods of volcanic quiescence but likely under  
184 the presence of hydrothermal activity. They are often interbedded with layers of composite carbonaceous  
185 grains, which Walsh (1992) compared to globular bacterial colonies or organic aggregates, however, the  
186 biogenicity of these grains still needs to be further established (Trower and Lowe, 2016). In the following,  
187 reported microbial mats and biofilms from the Middle Marker, the Buck Reef Chert, and Josefsdal Chert  
188 will be described in more detail.

#### 189 190 **4.1.1 Middle Marker**

191 The 3.472 Ga Middle Marker (H1) at the base of the Hooggenoeg Formation represents the oldest, relatively  
192 unmetamorphosed sedimentary unit of the BGB (Lanier and Lowe, 1982; Armstrong et al., 1990). It has a  
193 thickness of 3 to 6 m and is composed of silicified komatiitic ash and fine layers of relatively pure  
194 carbonaceous cherts that contain composite grains and carbonaceous wisps of proposed biogenic origin  
195 (Lanier and Lowe, 1982; Walsh, 1992; Lowe, 1999; Walsh and Lowe, 1999). Deposition occurred likely  
196 on a flat, tide- or wave influenced shelf in water depths of several 10s to 100 m (Byerly et al., 2019).  
197 Fine, crinkly laminations, interbedded with the volcanoclastic sand- and siltstones of this unit, have been  
198 interpreted as fossil microbial mats by Hickman-Lewis et al. (2018), mainly based on their carbonaceous  
199 composition, micro-tufted morphology, sediment trapping and cohesive behavior, and the occurrence of  
200 wisp-like structures, interpreted as erosional mat (Fig. 3A and B). The carbonaceous laminations occur in  
201 packets of 200  $\mu\text{m}$  to 2.5 mm thickness, contain detrital quartz and volcanic grains, and generally have a  
202 low surficial relief, which is described by the authors as micro-tufted (Fig. 3A and B). These crinkly, micro-  
203 tufted structures ( $<100\mu\text{m}$  in height) of proposed primary biogenic origin can be distinguished from pseudo-  
204 tufted structures (up to 0.8 mm in height) that formed secondary as a result of plastic deformation triggered  
205 by the settling of dense particles (Fig. 3C and D; Hickman-Lewis et al., 2018). The micro-tufted structures

337  
338  
339  
340  
341  
342  
343  
344  
345  
346  
347  
348  
349  
350  
351  
352  
353  
354  
355  
356  
357  
358  
359  
360  
361  
362  
363  
364  
365  
366  
367  
368  
369  
370  
371  
372  
373  
374  
375  
376  
377  
378  
379  
380  
381  
382  
383  
384  
385  
386  
387  
388  
389  
390  
391  
392

206 were further used by Hickman-Lewis et al., (2018) to tenta  
207 were formed by anoxygenic phototrophs. However, it is hard to constrain the microbial metabolism relying  
208 on mat morphology alone, especially if it is only of minor topographic relief and secondary deformation  
209 structures are present. More valuable insights into the metabolism(s) of the Middle Marker mats could be  
210 gained from the analysis of organic carbon isotopes, which would also help to further strengthen their  
211 biogenicity.

212

#### 213 **4.1.2 Buck Reef Chert**

214 The 3.416 Ga Buck Reef Chert (K1) is a 250–400-m-thick unit of carbonaceous and ferruginous cherts at  
215 the base of the Kromberg Formation, exposed continuously along nearly 50 km of strike in the west limb  
216 of the Onverwacht Anticline (Kröner et al., 1991; Lowe and Worrell, 1999). A correlative section in the  
217 east limb of the Onverwacht Anticline comprises three 10–25-m-thick chert units (Kc1, Kc2, Kc3), that are  
218 interbedded with basalt flows (Walsh, 1992; Lowe and Byerly, 1999). The cherts are thought to be of  
219 primary origin and likely precipitated from normal marine water, which was saturated with respect to  
220 amorphous silica during the Archean (Lowe, 1999b; Knauth and Lowe, 2003; Tice and Lowe, 2006a) rather  
221 than from hydrothermal fluids (de Wit et al., 1982; Westall et al., 2001). Sediments of the Buck Reef Chert  
222 were deposited on subsiding open-marine volcanic platform and can be subdivided in three main  
223 depositional facies (basal evaporitic, middle platform, and deep basin), which reflect deposition under  
224 successively deeper-water conditions (Tice and Lowe, 2004). The silicified evaporites from the evaporitic  
225 facies, were originally interpreted as remnants of nahcolite (Lowe and Worrell, 1999) but may represent  
226 pseudomorphs after aragonite (Otálora et al., 2018). Fine anastomosing carbonaceous laminations (Fig. 4A-  
227 F) and in places ripped up, plastically deformed rolled-up fragments (Fig. 5 A and B), occurring within  
228 black bands in black-and-white banded cherts of the platform facies, were interpreted as remnants of  
229 cohesive microbial mats (Walsh and Lowe, 1999; Tice and Lowe, 2004, 2006a, 2006b; Tice, 2009; Tice et  
230 al., 2011). The mats were once thriving in shallow-water, photic zone paleoenvironments below fair-  
231 weather wave base and show three distinct mat morphotypes: (1) alpha-type, fine carbonaceous laminations  
232 that incorporate and loosely drape detrital grains underlying detrital grains and form silica-filled lenses (Fig.  
233 4A and B); (2) beta-type, fine meshworks of filament-like strands (<5µm in diameter), which drape  
234 underlying detrital grains (Fig. 4C and D); and (3) gamma-type, evenly spaced flat laminations that tightly  
235 drape underlying sediments (Fig. 4E and F; Tice, 2009). The formation of different mat morphotypes is  
236 thought to be primarily controlled by local variations in ambient light intensity and/or current energy.  
237 Consequently, the first two morphotypes (alpha and beta) probably formed in shallower water, which is  
238 also supported by their more complex morphology and association with coarser-grained sediments (Tice  
239 2009). Bulk organic carbon isotope measurements of the carbonaceous laminations, with  $\delta^{13}\text{C}_{\text{org}}$  values



393  
394  
395  
396  
397  
398  
399  
400  
401  
402  
403  
404  
405  
406  
407  
408  
409  
410  
411  
412  
413  
414  
415  
416  
417  
418  
419  
420  
421  
422  
423  
424  
425  
426  
427  
428  
429  
430  
431  
432  
433  
434  
435  
436  
437  
438  
439  
440  
441  
442  
443  
444  
445  
446  
447  
448

240 ranging between  $-36.9\%$  and  $-20.1\%$ , and a mean of  $-29.9\%$  ( $n = 19$ , Tice and Lowe 2006b), serve as  
241 additional evidence for a biogenic origin of the mats, which were formed by photosynthetic microbes that  
242 most likely applied hydrogen-based carbon fixation (Tice and Lowe, 2004a, 2006a). Raman  
243 microspectroscopic analysis further revealed that the carbonaceous matter preserved in the Buck Reef Chert  
244 has experienced sub- to lower-greenschist facies temperatures, consistent with regional peak metamorphic  
245 temperatures, and thus confirming its syngenetic origin (Tice et al., 2004; van Zuilen et al., 2007). Overall,  
246 the microbial mats preserved in the Buck Reef Chert represent one of the best documented evidence for  
247 ancient life in the Onverwacht Group. Future work could focus more on micro-scale investigations, increase  
248 the spatial resolution of organic carbon isotope measurements, and try to acquire also nitrogen isotope  
249 values in order to learn more about the biogeochemical cycling of these elements by the mat-forming  
250 microbial communities.

251

252

### 253 **4.1.3 Josefsdal Chert**

254 The Josefsdal Chert comprises a 6–30-m-thick succession of silicified volcanoclastic rocks, located in a  
255 fault-bounded sliver, and is considered to be the lateral equivalent of the 3.334 Ga Footbridge Chert (K3c;  
256 (Kröner et al., 1996; Lowe and Byerly, 1999) at the top of the Kromberg Formation (Hofmann and Bolhar,  
257 2007; Westall et al., 2015). Sedimentary structures, such as ripple marks, planar- and cross-lamination  
258 indicate that deposition likely occurred in tidal, nearshore environments under the influence of  
259 hydrothermal activity, which is supported by REE patterns with positive Eu and Y anomalies and was likely  
260 driven by the circulation of silica-saturated seawater through cooling basaltic lavas that occur  
261 stratigraphically below the Josefsdal Chert (Hofmann and Harris, 2008; Westall et al., 2011, 2015, 2018).  
262 Cracks, only a few  $\mu\text{m}$  in width, occurring in structures interpreted as fossil biofilms from these deposits,  
263 were further used to infer periods of subaerial exposure, desiccation, and evaporation (Westall et al., 2001;  
264 2006). Such cracks are, however, less suitable to reconstruct the depositional context, as they are only  
265 visible with the SEM (scanning electron microscope) and not in the outcrops. Altermann (2001) suggested  
266 that these cracks and the pseudomorphic evaporite minerals, as well as some putative rod-shaped  
267 microfossils (2–3.8 mm long and interpreted as remnants of sulphate-reducing bacteria) described by  
268 Westall et al. (2001, 2006) from these cherts, might represent sample preparation artefacts introduced  
269 during HF etching (Wacey, 2009). Moreover, the fact that the anions of the putative, often idiomorphic,  
270 evaporite crystals have been replaced by fluorine (Westall et al., 2006) further indicates that they could  
271 represent artefacts, especially as it has been shown that mineral artefacts such as fluorides and fluosilicates  
272 commonly form during HF etching (Karkhanis, 1977) and might mimic evaporitic minerals. A more  
273 promising candidate for life in these deposits are therefore the structures that are visible in petrographic

449  
450  
451  
452  
453  
454  
455  
456  
457  
458  
459  
460  
461  
462  
463  
464  
465  
466  
467  
468  
469  
470  
471  
472  
473  
474  
475  
476  
477  
478  
479  
480  
481  
482  
483  
484  
485  
486  
487  
488  
489  
490  
491  
492  
493  
494  
495  
496  
497  
498  
499  
500  
501  
502  
503  
504

274 thin section and resemble silicified biofilms and microbial mats (Fig 6 A-C). The microbial mat-like  
275 structures occur in banded black and white cherts as layered packets, 100–1000  $\mu\text{m}$  thick, that are composed  
276 of  $\sim 10\mu\text{m}$  thin, wavy carbonaceous biofilms with incorporated fine-grained detrital volcanic clasts and  
277 quartz grains (Westall et al., 2006; 2011; 2015). Torn and plastically deformed fragments of these biofilms  
278 occur partially peeled of below and above distinct mat horizons, which is interpreted as evidence for  
279 contemporaneous (lateral?) injection of hydrothermal fluids (Fig. 6D, Westall et al., 2015). A single biofilm  
280 (1–4  $\mu\text{m}$  thick) exposed on fresh fractured bedding surface has been extensively studied by Westall et al.  
281 (2001, 2006, 2011; sample 96SA05) and SEM observations revealed the presence of multiple layers of  
282 parallel filament-like structures with constant diameter of 0.25  $\mu\text{m}$ , which are embedded in a granular to  
283 smooth film interpreted as extracellular polymeric substance. Carbonaceous clots, 50–500  $\mu\text{m}$  in diameter  
284 and interpreted as degraded remnants of chemosynthetic biomass, represent another proposed biosignature  
285 from Josefsdal Chert (Westall et al., 2015), however their biogenicity still needs to be further established.  
286 Two bulk organic carbon isotope measurements from the Josefsdal Chert show  $\delta^{13}\text{C}_{\text{org}}$  values of  $-22.7\text{‰}$   
287 (bulk sample, Westall, et al 2001) and  $-26.8\text{‰}$  (carbon-rich black layer, Westall et al., 2006). While *in situ*  
288 measurements of the carbonaceous biofilms yield  $\delta^{13}\text{C}_{\text{org}}$  values of  $-45\text{‰}$  to  $-13\text{‰}$  and a single  $\delta^{34}\text{S}$  value  
289 of  $-24\text{‰}$  (Westall et al., 2015). These values support a biogenic origin of the biofilms/mats and were further  
290 used to conclude that the latter were formed by anoxygenic photosynthesizers and sulphur reducing bacteria  
291 (Westall et al. 2011, 2015). Future *in situ* isotope studies on the organic remains in these samples should  
292 increase the amount of data points and aim to better document the analytical areas (see e.g. Williford et al.  
293 2013, 2016) in order to spatially resolve the large range of  $\delta^{13}\text{C}_{\text{org}}$  values, and to distinguish it from the  
294 background signal of the carbonaceous cherts, which might differ significantly, as documented by Oehler  
295 et al. (2017) for samples of the Buck Reef Chert that show  $\delta^{13}\text{C}_{\text{org}}$  values ranging between  $-47.1\text{‰}$  and  
296  $-24.0\text{‰}$ .

## 297 298 **4.2 Microfossils**

299 The positive identification of Archean microfossils is due to their often very simple morphology extremely  
300 challenging, several well-established criteria exist (see Schopf, 2004; Brasier et al., 2006; Wacey, 2009),  
301 while *in situ* carbon isotope analysis of individual microfossil candidates has become another required  
302 method for the evaluation of their biogenicity in recent years (e.g. House et al., 2013; Lepot et al., 2013;  
303 Williford et al., 2013, 2016). Putative microfossils in the carbonaceous cherts of the Onverwacht Group are  
304 extremely rare. The first systematic analysis of Walsh (1992) and Walsh and Lowe (1999) revealed that  
305 only 9 of more than 400 analyzed samples contained possible microfossils of filamentous, lenticular, and  
306 spheroidal shapes.

307

505  
506  
507  
508  
509  
510  
511  
512  
513  
514  
515  
516  
517  
518  
519  
520  
521  
522  
523  
524  
525  
526  
527  
528  
529  
530  
531  
532  
533  
534  
535  
536  
537  
538  
539  
540  
541  
542  
543  
544  
545  
546  
547  
548  
549  
550  
551  
552  
553  
554  
555  
556  
557  
558  
559  
560

308 **4.2.1 Filamentous structures**

309 Filamentous microstructures of carbonaceous composition were identified in a single 2 cm thick black-and-  
310 white banded chert layer in the upper Hooggenoeg Formation (Walsh and Lowe, 1985; Walsh 1992). These  
311 tread-like or cylindrical, unbranched filaments are solid, 0.2 – 2.5  $\mu\text{m}$  in diameter, up to 200  $\mu\text{m}$  long and  
312 occur associated with carbonaceous laminations interpreted as microbial mats. Although originally  
313 classified as possible microfossils Walsh (2000) noted that they may have formed abiotically and could  
314 thus represent simple mineral filaments (Wacey, 2009).  
315 More convincingly biological filaments occur associated with fossil mats in several localities of the Buck  
316 Reef Chert (K1 and K1c2; Byerly et al., 2019). The hollow cylindrical filaments, 1.2 – 1.4  $\mu\text{m}$  in diameter  
317 and 10 – 150  $\mu\text{m}$  in length, are composed of carbonaceous matter and fine pyrite (Fig. 7A-C). They mostly  
318 occur oriented subparallel to bedding or sometimes as interwoven, tangled clumps (Walsh and Lowe, 1985;  
319 Walsh 1992). These hollow, sheath-like filaments are similar in size and shape to modern filamentous  
320 bacteria and are of possible organic origin (Walsh 1992, Altermann, 2001), however, high-resolution  
321 petrographic and detailed *in situ* carbon isotope analysis would be desirable to further support this  
322 interpretation.

323  
324

325 **4.2.2 Lenticular structures**

326 Lenticular structures (previously named “spindle-shaped” structures) represent a group of enigmatic  
327 microfossils that are also well-known from the Pilbara Craton of Western Australia where their biogenicity  
328 is well established (e.g. Sugitani et al., 2007, 2010, 2013, Oehler et al., 2009, 2017; House et al., 2013;  
329 Kozawa et al., 2018). There, the lenticular objects occur individually or in groups or chains of several  
330 individuals. Lense- or, disk-shaped microstructures, 30–60  $\mu\text{m}$  in long axis, with hollow centers and  
331 carbonaceous walls have been first documented in the BGB by Pflug (1966, 1967) and Pflug et al., (1969)  
332 from cherts of the Fig Tree Group that were later assigned to the upper Onverwacht Group (Mendon  
333 Formation, previously named Swartkoppie Formation, (Schopf, 1975; Lowe and Knauth, 1977)). The  
334 structures gently taper towards the ends of their long axes, occur isolated or sometimes in groups of two or  
335 more specimens (Fig. 8A-D), which are connected at their poles, and were interpreted as the remains of  
336 thread-like bacterial colonies (Pflug, 1966, 1967). Walsh (1992) interpreted very similar lenticular  
337 structures, 13–135  $\mu\text{m}$  long and 4.5–61  $\mu\text{m}$  wide, from detrital layers above the basal evaporitic facies of  
338 the Buck Reef Chert (K1) as possible sheaths of colonies of bacterial cells or carbonaceous coatings around  
339 former gypsum crystals (Fig. 8E-H). A biological origin of the structures is supported by *in situ*  $\delta^{13}\text{C}_{\text{org}}$   
340 analysis that revealed values ranging between -39.3‰ to - 35.5 ‰, consistent with autotrophic carbon  
341 fixation (n = 8; Oehler et al., 2017). Based on their robust morphology, shallow water habitat and  $\delta^{13}\text{C}_{\text{org}}$

561  
562  
563  
564  
565  
566  
567  
568  
569  
570  
571  
572  
573  
574  
575  
576  
577  
578  
579  
580  
581  
582  
583  
584  
585  
586  
587  
588  
589  
590  
591  
592  
593  
594  
595  
596  
597  
598  
599  
600  
601  
602  
603  
604  
605  
606  
607  
608  
609  
610  
611  
612  
613  
614  
615  
616

342 values Oehler et al. (2017) proposed that the lenticular forms might represent microbes with a planktonic  
343 stage in their life cycle, making it to a very promising claim for microbial life in the BGB.

344

### 345 **4.2.3 Spheroidal structures**

346 Spheroidal microstructures of carbonaceous composition belong to a very common group of putative  
347 microfossils in the Onverwacht Group but the evaluation of their biogenicity is due to their simple  
348 morphology often very challenging.

349 Glikson et al. (2008) identified clusters of spheroidal, cell-like objects (2–10  $\mu\text{m}$  in diameter) with granular  
350 walls from cherts of the Hooggenoeg Formation (H3c and H5c), which display features of possible cell  
351 wall degradation (Fig. 9A and B). The spheroids are comparable with the modern hyperthermophilic  
352 *Methanocaldococcus jannaschii* and were thus interpreted as remnants of chemosynthetic microbes once  
353 thriving in a seafloor hydrothermal system. This is a promising sign for life, but follow-up studies should  
354 also document the sedimentological context, perform analysis on more than two samples, and include *in*  
355 *situ* isotope measurements (Wacey et al., 2009). Large granular-walled spheroids and ellipsoids (10–84  $\mu\text{m}$   
356 in length; Fig. 9C and D) and clusters of thin-walled spheroids (4.5–12.8  $\mu\text{m}$  in diameter; Fig. 9E and F)  
357 from the Buck Reef Chert were interpreted as probable microfossils of coccoidal bacteria or spores (Walsh,  
358 1992). However, these simple spheres may be produced abiotically in various ways and were therefore  
359 reinterpreted as abiotic self-organized structures, such as spherulitic chert (Brasier et al., 2006). Kremer  
360 and Kazmierczak (2017) reported spheroidal microstructures, 3–12  $\mu\text{m}$  in diameter, from the Buck Reef  
361 Chert (K1c2) and tentatively conclude that they may represent the variably degraded remains of coccoidal  
362 cyanobacteria (Fig. 9G and H). Although the cell-like objects occur in groups or clusters, preserved in black  
363 cherts with bulk  $\delta^{13}\text{C}_{\text{org}}$  values of  $-26.5\text{‰}$  and  $-24.3\text{‰}$  ( $n = 2$ ), their outer walls often have a more angular  
364 than rounded appearance, which resemble crystal terminations, thus making a biological origin less  
365 favorable (Hickman-Lewis, 2019). Alternatively, these objects might represent carbonaceous linings on  
366 replaced minerals or crystal rims (Brasier et al., 2006). Moreover, beyond morphological similarity, the  
367 positive identification of cyanobacteria and oxygenic photosynthesis hundreds of millions of years before  
368 most other evidence, requires independent geochemical evidence for the local presence of free oxygen,  
369 which is currently not available. Future studies should include nanoscale analysis of the putative cell walls  
370 and *in situ* isotope measurements.

371 Another occurrence of possible organic microspheres, 1– 4  $\mu\text{m}$  in diameter, has been described by Knoll  
372 and Barghoorn (1977) from the Msauli Chert (M1c; Mendon Formation, previously named Swartkoppie  
373 Formation (Lowe, 1999c)), which was deposited in shallow-water nearshore environments (Fig. 9I). These  
374 carbonaceous spheres occur as isolated or paired objects, are often flatten, wrinkled or folded, show a  
375 narrow unimodal size frequency distribution ( $n = 200$ ), evidence of possible cell division, and were

617  
618  
619  
620  
621  
622  
623  
624  
625  
626  
627  
628  
629  
630  
631  
632  
633  
634  
635  
636  
637  
638  
639  
640  
641  
642  
643  
644  
645  
646  
647  
648  
649  
650  
651  
652  
653  
654  
655  
656  
657  
658  
659  
660  
661  
662  
663  
664  
665  
666  
667  
668  
669  
670  
671  
672

376 interpreted as the remains of primitive prokaryotes (Knoll and Barghoorn, 1977). However, without any  
377 geochemical analysis also these structures cannot be unambiguously identified as biological (Wacey, 2009).

378

379

### 380 **4.3 Stromatolites**

381 Compared to its Australian counterpart the currently known stromatolite occurrences in the BGB are very  
382 rare. Byerly et al. (1986) reported putative pseudocolumnar stromatolites that crop out for more than 10 km  
383 along strike in grey to black cherts assigned to member M2c of the ~3.23 Ga Mendon Formation (Walsh,  
384 2004; Lowe and Byerly, 2015), which is interbedded with komatiitic lava flow deposits. [Note that these  
385 outcrops were initially assigned to the Fig Tree Group (Byerly et al., 1986), but are now thought to belong  
386 to the Mendon Formation in the upper Onverwacht Group (Lowe, 1994)]. The possible stromatolites occur  
387 in layers of <1 to 20 cm thickness and display variable morphologies, ranging between low-relief,  
388 asymmetrical, sometimes laterally-linked domes (1–3 cm wide and 0.5–3 cm high), rare pseudocolumns  
389 with bridging laminae (up to 10 cm height), and crinkly stratiform laminations (50–100 μm thick; Fig. 10A  
390 and B). Individual laminae are composed of minor amounts of primary carbonaceous matter and variable  
391 amounts of secondary, fine-grained, often idiomorphic tourmaline minerals (sometimes up to 50%), which  
392 may have been derived through the hydrothermal remobilization of previously formed, boron-rich  
393 evaporites (Fig. 10C; Byerly and Palmer, 1991). Alternatively, the tourmaline mineralization could have  
394 been caused by heating and partial ocean evaporation related to a large asteroid impact recorded by spherule  
395 beds S5 and S8, which occur associated with some of the stromatolites (Lowe and Byerly, 2015).  
396 Conglomerates composed of laminated silica chips occur in the throughs between stromatolite domes and  
397 have been interpreted as fragments of eroded stromatolites or sinter crusts, likely deposited in the aftermath  
398 of a large impact (Fig. 10D). Similar stromatolite-crust chip conglomerates have also been reported from  
399 the Fig Tree Group (Sheba Formation) where they are overlain by spherule bed S5 (Lowe and Byerly, 2015,  
400 2018). The stromatolitic structures were possibly formed by hyperthermophilic microbial communities in  
401 shallow-water depositional environments during periods of relative volcanic quiescence and likely  
402 experienced the profound effect of distant asteroid impacts (Byerly et al., 1986; Lowe and Byerly, 2018).  
403 The widespread occurrence, morphological variability, and similarity to other fossil and modern  
404 stromatolites suggest a biogenic origin of these structures (Awramik, 1992). However, organic carbon  
405 isotope measurements, three-dimensional morphological investigations, a better documentation of the  
406 different morphotypes (Allwood et al., 2006), combined with high-resolution petrographic analysis, and a  
407 clear distinction from possibly abiogenic hot-spring silica crust precipitates (Lowe, 1994) would be  
408 desirable to further support this interpretation.

409

673  
674  
675 410  
676 411  
677  
678 412  
679 413  
680 414  
681 415  
682 416  
683 417  
684 418  
685 419  
686 420  
687 421  
688 422  
689 423  
690 424  
691 425  
692 426  
693 427  
694 428  
695 429  
696 430  
697 431  
698 432  
699 433  
700 434  
701 435  
702 436  
703 437  
704 438  
705 439  
706 440  
707 441  
708 442  
709 443  
710  
711  
712  
713  
714  
715  
716  
717  
718  
719  
720  
721  
722  
723  
724  
725  
726  
727  
728

## 5. The ~3.22 Ga Moodies Group

The ca. 3.22 Ga Moodies Group is the uppermost stratigraphic unit of the BGB and represents the world's oldest well-preserved alluvial to shallow-marine tidal deposit. It consists of a up to 3.5 km thick succession of quartz-rich sandstones with subordinate conglomerates, mudstones, siltstones, thin volcanic tuff beds, minor banded iron formations and a basaltic lava, deposited in marine (deltaic, inter-, and subtidal) and terrestrial (alluvial, fluvial, possibly aeolian) paleoenvironments (Hall, 1918; Visser, 1956; Anhaeusser, 1976; Eriksson, 1977, 1979, Heubeck and Lowe, 1994a, 1999; Simpson et al., 2012; Homann et al., 2015, 2018; Heubeck et al., 2016). The age of the Moodies Group is tightly constrained by Uranium–lead dating of single-zircons from several dacitic tuffs and rare felsic dykes, which indicate that deposition began about  $3.223 \pm 1$  Ga and had ended by about  $3.219 \pm 9$  Ga (De Ronde and Kamo, 2000; Heubeck et al., 2013). Moodies strata north of the Inyoka Fault are preserved in several, commonly northward-overturned synclines that are tectonically separated by major faults (Fig. 2). These deposits not only contain a large variety of well- preserved sedimentary structures, they also offer a high-resolution archive of Paleoproterozoic surface and sedimentation processes, as well as a unique window into a widespread, diverse and well adapted microbial ecosystem. Reported biosignatures from the Moodies Group include intertidal and fluvial microbial mats, silicified remnants of cavity-dwelling microorganisms (coelobionts), and large organic-walled microfossils (acritarchs), as detailed below.

### 5.1 Microbial mats

Fossil microbial mats in the Moodies Group have been identified so far in intertidal deposits of the Saddleback Syncline and in alluvial-fluvial deposits of the Dycedale Syncline (Fig. 11A-C). In the Saddleback Syncline the mats are preserved as carbonaceous, crinkly laminations (0.5–1 mm thick), interbedded with medium- to coarse-grained sandstones, and associated with desiccation cracks (Fig. 12A) They represent the oldest known examples of siliciclastic tidal mats in the geological record (Noffke et al., 2006; Heubeck, 2009; Gamper et al., 2012; Homann et al., 2015). These mats draped and stabilized horizontally laminated and rippled sandstones, and show an enrichment in fine-grained quartz and feldspar, as well as heavy mineral grains (zircon and rutile or anatase), likely caused by microbial baffling and trapping, which is a commonly observed in epibenthic microbial mats (Gerdes et al., 2000). Microbial-mat-associated structures such as eroded mat fragments (mat chips), macroscopic tufts, shrinkage cracks, silicified gas domes and lenses, and subvertical fluid-escape structures are indicative for a former cohesive consistency and very common features in these deposits supporting the biogenic origin of the mats (Fig. 12B-D; Heubeck, 2009; Homann et al., 2015, 2016, 2018), while microbial wrinkle structures previously reported by Noffke et al. (2006) have not been observed in any of the follow-up studies. A detailed study

729  
730  
731  
732  
733  
734  
735  
736  
737  
738  
739  
740  
741  
742  
743  
744  
745  
746  
747  
748  
749  
750  
751  
752  
753  
754  
755  
756  
757  
758  
759  
760  
761  
762  
763  
764  
765  
766  
767  
768  
769  
770  
771  
772  
773  
774  
775  
776  
777  
778  
779  
780  
781  
782  
783  
784

444 of the sedimentological and paleoenvironmental context of these fossil mats revealed that they are laterally  
445 traceable for ~15 km in a ~1000 m-thick succession in the lower part of the Saddleback Syncline and show  
446 distinct morphological adaptations to different hydrodynamic settings: (1) planar-type in coastal floodplain,  
447 (2) wavy-type in intertidal, and (3) tufted-type in upper inter- to supratidal facies (Homann et al., 2015).  
448 Such facies dependent changes in the prevalent mat morphotypes are to be expected in a dynamic, tidally-  
449 influenced coastal environment and serve as an additional biogenicity indicator (Allwood et al., 2006;  
450 Brasier et al., 2006). Moreover, the widespread occurrence of these fossil mats is consistent with a primary,  
451 microbially mediated, cohesive erosion-resistant relief on the paleosurface that was locally deformed by  
452 migrating gases and fluids, and in places eroded and incorporated in mat-chip conglomerates.  
453 Based on the restriction of the mats to shallow-water, photic zone environments and their apparent absence  
454 in subtidal settings, it is very likely that they were formed by phototrophic microbial communities (Noffke  
455 et al., 2006; Heubeck, 2009, Homann et al., 2015). In fact, the Moodies microbial mats show some striking  
456 morphological similarities to modern cyanobacterial mats e.g. from Bahar Alouane, Tunisia (Fig. 12A-D;  
457 Gerdes et al., 2000; Gerdes, 2007), Shark Bay, Australia (Jahnert and Collins, 2013), 2013), Texas Gulf  
458 Coast, USA (Bose and Chafetz, 2009), and the Red Sea of Saudi Arabia (Taj et al., 2014). Especially the  
459 occurrence of mats with macroscopic, 0.3-to-1 cm-high tufts that closely resemble tufted mats build by  
460 filamentous cyanobacteria (Fig. 12C), led to the conclusion that the tufted mats of the Moodies Group were  
461 perhaps build by ancestral cyanobacteria (Homann et al., 2015). Even tough, no geochemical data  
462 supporting the local presence of free oxygen (and thus oxygenic photosynthesis) at 3.22 Ga have been found  
463 so far in the Moodies Group, fossil evidence indicative for ancient gas production, accumulation, and  
464 migration is plentiful in the near vicinity of the mats. Now chert-filled cavities in the interior of some tufts  
465 likely represent silicified gas bubbles that were trapped within the mat fabric, which is a common feature  
466 in cyanobacterial mats that produce oxygen-rich bubbles with strikingly similar morphologies (Fig. 12C;  
467 Bosak et al., 2010; Homann et al., 2015). Other types of silicified cavities include domes and bedding  
468 parallel lenses beneath the fossil mats that either formed through accumulation of gases produced by  
469 metabolic activity, due to the decay of organic matter, or alternatively by tidal-driven hydraulic pumping  
470 of the ambient air trapped in pore space (Figs. 12D and 14; Homann et al., 2016). Some of these cavities  
471 where also inhabited by microbial communities (see below in 5.2).  
472 Besides the main mat occurrence in the tidal marine deposits of the Saddleback Syncline, fossil microbial  
473 mats also have been identified in the Dycedale Syncline (Homann et al., 2018), where a large variety of  
474 sedimentary structures indicates that this succession records a transition from alluvial-fluvial (terrestrial) to  
475 tide-influenced marine sedimentation (Heubeck and Lowe, 1994; Eriksson et al., 2006; Heubeck et al.,  
476 2016). These terrestrial mats occur confined to fluvial deposits at the base of a transgressive sequence that  
477 gradually deepens upward through deltaic, and medium-energy tidal, into subtidal siliciclastic deposits.

785  
786  
787  
788  
789  
790  
791  
792  
793  
794  
795  
796  
797  
798  
799  
800  
801  
802  
803  
804  
805  
806  
807  
808  
809  
810  
811  
812  
813  
814  
815  
816  
817  
818  
819  
820  
821  
822  
823  
824  
825  
826  
827  
828  
829  
830  
831  
832  
833  
834  
835  
836  
837  
838  
839  
840

478 They are interbedded with gravely sandstones, drape conglomerate beds, are plastically deformed by 10-  
479 to 50-cm-high fluid-escape structures, and commonly experienced periods of subaerial exposure and  
480 desiccation evidenced by associated desiccation cracks (Fig. 13A and B). The terrestrial microbial mats of  
481 the Dycedale Syncline currently represent the oldest direct fossil trace for life on land (Homann et al.,  
482 2018). Overgrowth rims in pyrites from Moodies Group paleosols show signs of biogenic sulfur  
483 fractionation ( $\delta^{34}\text{S}_{\text{VCDT}}$  values between  $-20\text{‰}$  and  $-24.5\text{‰}$ ) and provide additional geochemical evidence  
484 for the presence of a Paleoarchean terrestrial biosphere (Nabhan et al., 2016a, b). Compared to the marine  
485 mats the carbonaceous laminae of terrestrial mats are similarly well preserved, but with up to 4 mm of  
486 preserved thickness often thicker than their marine counterparts (Fig. 11A and B; Fig. 13C). They are  
487 composed of a dense meshwork of interwoven filament-like microstructures that envelop fine-grained  
488 detrital particles whose long axes are preferentially aligned parallel to bedding (Fig. 13D and E; Homann  
489 et al., 2018). Individual carbonaceous filamentous structures are 1–3  $\mu\text{m}$  in diameter and resemble modern  
490 biofilm-forming, filamentous microorganisms. In places, a notable enrichment of tourmaline minerals can  
491 be observed in the mat fabric, which has also been reported from the stromatolitic laminae of the Mendon  
492 Formation (Byerly et al., 1986; Byerly and Palmer, 1991) and might be driven by evaporitic processes, but  
493 certainly demands further investigations. Raman spectroscopic analyses confirmed that both the terrestrial  
494 and marine mats are composed of organic carbon that has experienced similar peak temperatures of  $\sim 365^\circ\text{C}$ ,  
495 consistent with the metamorphic grade of the Moodies Group (Xie et al., 1997; Tice et al., 2004) and thus  
496 demonstrating their synsedimentary origin and biogenicity (Homann et al., 2018). A detailed study of  
497 Homann et al. (2018) documented a significant difference in the biogeochemical cycling of carbon and  
498 nitrogen in terrestrial and marine mats. The preserved organic matter in the terrestrial mats shows  $\delta^{13}\text{C}_{\text{org}}$   
499 values ranging between  $-23.6\text{‰}$  and  $-17.9\text{‰}$  (mean =  $-21.2\text{‰}$ ;  $n = 36$ ) and  $\delta^{15}\text{N}$  values between  $+1.9\text{‰}$   
500 and  $+5.6\text{‰}$  (mean =  $+4.3\text{‰}$ ;  $n = 10$ ), in contrast to marine mats that show  $\delta^{13}\text{C}_{\text{org}}$  values ranging between  
501  $-33.9\text{‰}$  and  $-21.3\text{‰}$  (mean =  $-27.4\text{‰}$ ;  $n = 30$ ) and  $\delta^{15}\text{N}$  values between  $-0.7\text{‰}$  and  $+3.1\text{‰}$  (mean =  
502  $+1.8\text{‰}$ ;  $n = 10$ ). This  $\delta^{13}\text{C}_{\text{org}}$  composition of the terrestrial mats is consistent with autotrophic carbon  
503 fixation through the Calvin–Benson cycle, while  $\delta^{13}\text{C}_{\text{org}}$  values of the marine mats are best explained by  
504 carbon fixation via the Wood–Ljungdahl pathway, which includes acetogenic bacteria, methanogens and  
505 sulfate reducers. The observed trend in the Moodies Group microbial mats with  $\delta^{15}\text{N}$  values from as low as  
506  $-1\text{‰}$  (marine) to up to  $+5\text{‰}$  (terrestrial) likely reflects increasing fixed-nitrogen (i.e., nitrate, nitrite or  
507 ammonium) and conversion to  $\text{N}_2\text{O}/\text{N}_2$  in the terrestrial habitats, which further suggests that they possessed  
508 a fundamentally different respiratory community at depth in the mat, one that must have been sufficiently  
509 oxygenated for aerobic Nitrogen cycling (Ader et al., 2016; Stüeken et al., 2016). Alternatively, the  
510 contrasting nitrogen isotope compositions between terrestrial and marine settings could be related to a



841  
842  
843  
844  
845  
846  
847  
848  
849  
850  
851  
852  
853  
854  
855  
856  
857  
858  
859  
860  
861  
862  
863  
864  
865  
866  
867  
868  
869  
870  
871  
872  
873  
874  
875  
876  
877  
878  
879  
880  
881  
882  
883  
884  
885  
886  
887  
888  
889  
890  
891  
892  
893  
894  
895  
896

511 constant flux of atmospherically-fixed nitrogen on the early land surface that was probably too diffuse to  
512 be a significant source of fixed nitrogen to the marine biosphere (Homann et al., 2018).

513

## 514 **5.2 Cavity-dwelling life**

515 Lens-shaped, laterally tapering cavities, up to tens of centimeters in width and <0.5 cm in height, frequently  
516 occur beneath fossil microbial mat in intertidal deposits of the Saddleback Syncline (Fig. 14A; Homann et  
517 al., 2016). The silicified cavities resemble gas-filled, fenestral hollows in modern coastal environments that  
518 commonly form beneath cohesive, impermeable microbial mats and mat-bound sediments (Gerdes et al.,  
519 2000; Schieber et al., 2007). Due to the presence of carbonaceous laminations and wisps these chert lenses  
520 were initially interpreted as partially silicified epibenthic microstromatolites or thick mucilaginous mats  
521 (Heubeck 2009; Gamper et al., 2011), however, Homann et al. (2016) reported the additional presence of  
522 pendant columnar microstromatolites attached to the ceilings of former cavities and concluded that they  
523 must have accreted downwards in an open void space of synsedimentary origin (Fig. 14B-E). This gravity-  
524 oriented geometry and the downward-accretionary growth habit is well known from cavity-dwelling  
525 microorganisms (coelobionts; Kobluk and James, 1979; Jakubowicz et al., 2014), which have also been  
526 reported from synsedimentary cavities beneath microbial mats in sandstones of the Neoproterozoic Fortescue  
527 Group in Australia (Rasmussen et al., 2009). In places, sub-circular to ovoid-shaped fenestrae (~500 µm in  
528 diameter) that resemble trapped gas bubbles occur wedged between the carbonaceous laminae (Fig. 14C).  
529 SEM observations of the cavity-filling cherts reveal the presence of: (1) polygonal structures after HF  
530 etching for 28 days, interpreted as remnants of extracellular polymeric substance (EPS, Gamper et al.,  
531 2012), and (2) a meshwork of interwoven filamentous molds of likely biogenic origin that is completely  
532 embedded in the chert (Fig. 14F; unetched samples, Homann et al., 2016). The non-branching filaments  
533 (0.3–0.5 µm in diameter, n = 180) display a subdivision in regularly spaced, ~2-µm- long, rod-shaped  
534 segments and have a tubular morphology in cross section (Fig. 14G and H). Bulk carbon isotope  
535 measurements of the chert-bearing sandstones show  $\delta^{13}\text{C}_{\text{org}}$  values between -23.8‰ and -14.1‰ (mean =  
536 -20.5‰, n = 15; Gamper et al., 2012), however, *in situ* measurements of the carbonaceous laminae within  
537 the chert-cemented cavities yield  $\delta^{13}\text{C}_{\text{org}}$  values ranging between -32.3‰ and -21.3‰ (mean = -26.5‰; n  
538 = 12) that are probably more representative. These values are consistent with a purely chemotrophic or a  
539 photosynthetic community of coelobionts and support the biogenicity of the oldest evidence for cavity-  
540 dwelling life on Earth (Homann et al., 2016). Moreover, these findings support the view the cavities were  
541 among the first ecological niches to have been occupied by early microbial communities.

542

543

## 544 **5.3 Organic-walled microfossils**

897  
898  
899  
900  
901  
902  
903  
904  
905  
906  
907  
908  
909  
910  
911  
912  
913  
914  
915  
916  
917  
918  
919  
920  
921  
922  
923  
924  
925  
926  
927  
928  
929  
930  
931  
932  
933  
934  
935  
936  
937  
938  
939  
940  
941  
942  
943  
944  
945  
946  
947  
948  
949  
950  
951  
952

545 Carbonaceous spheroidal microstructures, 31–300  $\mu\text{m}$  in diameter (mean=122  $\mu\text{m}$ , n=98), have been  
546 identified in bedded siltstones and shales from underground drill cores that were assigned to the Clutha  
547 Formation and drilled 600m below the surface in the Agnes gold mine, Moodies Hills Block (Javaux et al.,  
548 2010). The carbonaceous structures are visible in petrographic thin sections and resistant to extraction via  
549 acid maceration (Fig. 15A-D). They show wrinkled and folded textures, a ~160-nm-thick wall with a  
550 homogenous ultrastructure and were interpreted as flattened, hollow, and partially degraded, organic-walled  
551 vesicles with preserved cell lumen (Fig. 15E-F; Javaux et al., 2010). Bulk carbon isotopes measurements  
552 show a large spread in  $\delta^{13}\text{C}_{\text{org}}$  values ranging between -16.4% and -28.3%, with an average of -22.4%  
553 (n=22), but no difference in the  $\delta^{13}\text{C}_{\text{org}}$  values between samples with and without microfossils has been  
554 observed. Consequently, such bulk measurements might not be very useful in constraining the biogenicity  
555 of the microstructures, however their carbonaceous composition and syngenetic origin is supported by  
556 Raman microspectroscopy. Based on their taphonomy and for the Paleoproterozoic uncommonly large size,  
557 Javaux et al. (2010) and Buick (2010). Javaux et al. (2010) concluded that the organic-walled microfossils  
558 might either represent remnants of extinct prokaryotes, colonial envelopes of cyanobacteria, or even  
559 eukaryotes. To unravel the biological affinity of these acritarchs remains the task for future investigations,  
560 which should ideally also aim to identify the microstructures in outcrop samples in order to further constrain  
561 their habitat and explore their possible relationship with the widespread, shallow-water microbial mats of  
562 the Moodies Group.

## 564 **6. Discussion**

### 566 **6.1 Evidence of Paleoproterozoic life in the BGB and comparison to the PGBs**

567 Traces of ancient life in the BGB occur mainly confined to bedded, carbonaceous cherts of the Onverwacht  
568 Group and the siliciclastic deposits of the Moodies Group. Preserved biosignatures in these deposits include  
569 putative microfossils of filamentous, spheroidal, and lenticular shape, stromatolites, and microbial mats.  
570 Filamentous microfossils occur very rarely in cherts of the Onverwacht Group but their biogenicity remains  
571 equivocal (Walsh and Lowe, 1985; Walsh 1992, 2010). The rod-shaped filamentous molds preserved in  
572 early silicified, syndepositional cavities of the Moodies Group resemble in shape and size microbial  
573 filaments and also their depositional context, beneath intertidal microbial mats, supports a biogenic origin  
574 (Homann et al., 2016). Spheroidal microstructures with carbonaceous walls, resembling coccoidal cells,  
575 belong to the most common group of putative microfossils in the Onverwacht Group but the assessment of  
576 their biogenicity is in most cases extremely challenging due to their simple, often symmetrical morphology  
577 that can be easily generated abiogenetically in form of e.g. fluid inclusions, vesicles, and spheroidal  
578 crystallites (Schopf and Walther 1983; Brasier et al., 2006). Solely, the spheroidal, cell-like objects reported

953  
954  
955  
956  
957  
958  
959  
960  
961  
962  
963  
964  
965  
966  
967  
968  
969  
970  
971  
972  
973  
974  
975  
976  
977  
978  
979  
980  
981  
982  
983  
984  
985  
986  
987  
988  
989  
990  
991  
992  
993  
994  
995  
996  
997  
998  
999  
1000  
1001  
1002  
1003  
1004  
1005  
1006  
1007  
1008

579 by Glikson et al. (2008) from the Hooggenoeg Formation and the large, organic-walled spheroids described  
580 by Javaux et al. (2010) from the Moodies Group have a well-established biogenicity. However, the  
581 biological affinity of the latter and the reason for their unusually large size currently remains unknown.  
582 Lenticular structures preserved in the Buck Reef Chert (Walsh 1992; Oehler et al., 2017) and probably also  
583 other cherts of the upper Onverwacht Group (Pflug 1966, 1967; Pflug et al., 1969) belong to the earliest  
584 reported and currently best studied microfossils in the BGB. Remains of these, likely planktonic,  
585 microorganisms have also been reported from the 3.45 Ga Strelley Pool Formation and the ~3 Ga Farrel  
586 Quartzite in the Pilbara Craton where their biogenicity is reasonably well established (e.g. Oehler et al.,  
587 2009, 2017; Sugitani et al. 2007, 2010, 2013; House et al., 2013; Kozawa et al., 2018). The morphologically  
588 similar specimens from Australia occur in the same depositional context and show strikingly similar mean  
589  $\delta^{13}\text{C}_{\text{org}}$  values ( $-37.0\%$  and  $-36.1\%$ ) in comparison to their South African counterparts with a mean  $\delta^{13}\text{C}_{\text{org}}$   
590 value of  $-37.3\%$  (Oehler et al., 2017). Abiogenic models for the formation of similar-looking structures  
591 derived from reworked vesicular volcanic glass exists (Wacey et al., 2018a, 2018b), however these pseudo-  
592 fossils do not resemble the same morphological and microstructural complexity (Alleon et al., 2018;  
593 Kozawa et al., 2018). Nevertheless, the occurrence of such pseudo-fossil examples highlights again the  
594 paramount importance of detailed micro- and nanoscale analysis in the evaluation of the biogenicity of  
595 putative microfossils. Additionally, future studies of microfossil-bearing cherts of the Onverwacht Group  
596 should always be accompanied by detailed analysis of the stratigraphic context and depositional facies, in  
597 combination with *in situ* geochemical analysis of the microfossils themselves and their encasing mineral  
598 matrix.

599 Stromatolites, generally considered as the most ancient macroscopically-visible traces for life on Earth, are  
600 surprisingly rare and currently not as well documented in the BGB in comparison to the PGBs, where the  
601 oldest unequivocal biogenic examples occur preserved in the 3.45 Ga Strelley Pool Formation (Allwood,  
602 et al 2006) and possibly also in the 3.48 Ga Dresser Formation (Fig. 16; Walter et al., 1980; Van  
603 Kranendonk et al., 2008). However, the often morphological very simple, laminated, domal to conical  
604 structures of Archean stromatolites can be easily confused with secondary abiogenic structures, especially  
605 in the absence of indicative microfossils. A recent study of Allwood et al. (2018), highlighting the  
606 importance of morphological analysis in combination with geochemistry at appropriate scales, serves as a  
607 cautionary tale and strongly questions the biogenicity of previously reported putative stromatolites from  
608 3.7 Ga old metacarbonate rocks of Greenland (Nutman et al., 2016). Compared to the greenstone belts in  
609 the Pilbara region, the documented deposit of the BGB contain only minor evidence of early carbonate  
610 environments, which is probably related to the predominance of volcanic and clastic deposition in  
611 combination with high sedimentation rates that made the conditions for stromatolite formation less  
612 favorable.

1009  
1010  
1011 613 The most widespread, pervasive, and probably also oldest trace of ancient life in the BGB are the remnants  
1012 614 of shallow-water microbial mats and biofilms. Mat-like laminations occur in almost all black-and-white-  
1013 615 banded, carbonaceous cherts of the Onverwacht Group (Walsh 1992), but only the examples reported from  
1014 616 the 3.472 Ga Middle Marker (Hickman-Lewis, et al, 2018), the 3.416 Ga Buck Reef Chert (Walsh and  
1015 617 Lowe, 1999; Tice and Lowe, 2004a, 2006a, b; Tice, 2009; Tice et al., 2011), and the 3.334 Ga Josefsdal  
1016 618 Chert (Westall et al., 2011, 2006, 2011, 2015) are reasonably well studied to support their biogenic origin.  
1017 619 Especially the mats and microfossils preserved in the up to 400-m-thick Buck Reef Chert represent a  
1018 620 particularly widespread (~50 km along strike), well-preserved and -documented record of the Paleoproterozoic  
1019 621 life. Besides the necessity to carefully reinvestigate more potentially microfossil- and mat-bearing  
1020 622 carbonaceous cherts in the BGB it is also crucial to further support the already existing claims for early life  
1021 623 from these units with more detailed geochemical analysis such as e.g. carbon, nitrogen, and sulphur isotope  
1022 624 data. The microbial mats preserved in the tidal and fluvial sandstones and conglomerates of the 3.22 Ga  
1023 625 Moodies Group are unique and currently not known from equivalent deposits from Australia (Fig. 16;  
1024 626 Noffke et al., 2006; Heubeck, 2009; Gamper et al., 2012; Homann et al., 2015, 2018). The quality of  
1025 627 preservation of the delicate carbonaceous mat laminae, distinct morphotypes, and mat-associated cavities  
1026 628 in these coarse-grained and gravely siliciclastic deposits is truly exceptional and implies a rapid fossilization  
1027 629 driven by early diagenetic silicification of the sediments (Heubeck 2009; Homann et al., 2015). The  
1028 630 observed difference in the biogeochemical cycling of carbon and nitrogen in tidal marine and fluvial  
1029 631 microbial mats from the Moodies Group (Homann et al., 2018) has demonstrated the potential of detailed  
1030 632 geochemical analysis, which can give valuable insights in the different carbon fixation pathways and  
1031 633 ultimately helps to constrain the metabolism(s) of the mat-building microbial communities and should  
1032 634 consequently also be applied more extensively to the mats preserved in the Onverwacht Group.  
1033  
1034  
1035  
1036  
1037  
1038  
1039  
1040  
1041  
1042  
1043  
1044

## 1045 636 **6.2 Habitats and paleoecology**

1046 637 Evidence for Paleoproterozoic life in the BGB have been reported from a wide range of paleoenvironments  
1047 638 including shallow marine (e.g. Byerly et al., 1986; Tice and Lowe, 2004a; Heubeck 2009; Homann et al.,  
1048 639 2015), fluvial (Homann et al., 2018), hydrothermal (Glikson et al., 2008; Westall et al., 2015), and possibly  
1049 640 planktonic settings (Walsh 1992; Oehler et al., 2017), as well as from cryptic cavities in the shallow  
1050 641 subsurface of intertidal deposits (Homann et al., 2016). Due to the general restriction of microbial mats to  
1051 642 shallow-water, photic zone paleoenvironments of the BGB, the common notion is that they were at least in  
1052 643 part composed of photosynthetic microbial communities and already had a high level of UV radiation  
1053 644 tolerance, while the microorganisms thriving in a hydrothermal context or in cavities were likely dominated  
1054 645 by chemotrophic communities. Nearly all of these early microbial communities must have been severely  
1055 646 affected by distant impacts of large asteroids (20 to 50 km in diameter), which occurred between 3.470 Ga  
1056  
1057  
1058  
1059  
1060  
1061  
1062  
1063  
1064

1065  
1066  
1067 647 and 3.225 Ga and are recorded in the BGB deposits by eight known ejecta layers (Fig. 2; Lowe and Byerly,  
1068 648 1986, 2018; Lowe et al., 1989). Besides impact-generated tsunamis it has been proposed that some of these  
1069 649 catastrophic events might have been large enough to cause partial boiling and sterilization of the oceans  
1070 650 and possibly triggered mass extinctions of low-temperature microbes, including most photosynthetic  
1071 651 microorganisms (Sleep et al., 1989; Lowe and Byerly, 2015). The question of how exactly early life  
1072 652 managed to survive these events or if the global ecosystem got entirely destroyed and biogenesis was reset  
1073 653 currently remains open.

1077 654 The Moodies Group ecosystem was particularly diverse, advanced, and well-adapted and includes large  
1078 655 spheroidal microfossils, Earth's earliest evidence of cavity-dwelling microbes (coelobionts), widespread  
1079 656 intertidal tufted microbial mats, laterally traceable for 15 km in a ~1000 m-thick succession, as well as  
1080 657 erosion-resistant fluvial microbial mats. The latter represent the oldest known direct fossil evidence for  
1081 658 terrestrial life on the continental surface and are ~500 Ma older than ~2.7 Ga old fluvio-lacustrine  
1082 659 stromatolites and coelobionts preserved in the Fortescue Group (Tumbiana and Hardey Formation,  
1083 660 Australia; Buick, 1992; Awramik and Buchheim, 2009; Rasmussen et al., 2009; Coffey et al., 2013) and  
1084 661 fluvial stromatolites documented in the Ventersdorp Supergroup (South Africa; Buck, 1980). Based on the  
1085 662 apparent morphological similarities between the shallow-marine microbial mats of the Moodies Group and  
1086 663 modern cyanobacterial mats such as e.g. macroscopic tufts, evidence for gas production and accumulation  
1087 664 in bubbles and domes, and their widespread occurrence and presumably fast growth rate, it has been  
1088 665 proposed that they were perhaps build by ancestral cyanobacteria (Homann et al., 2015). A recent molecular  
1089 666 clock study by Cardona et al. (2018) supports this interpretation and suggest that a primordial photosystem  
1090 667 capable of oxidizing water to oxygen could have formed before the most recent common ancestor of  
1091 668 cyanobacteria. Additionally, also the unusually large size of the organic-walled microfossils reported by  
1092 669 Javaux et al. (2010) indirectly suggests the requirement and the availability of oxygen at 3.22 Ga, although  
1093 670 no unequivocal geochemical signs for the local presence of free oxygen have been found so far in the  
1094 671 Moodies Group.

1103 672

## 1105 673 **7. Conclusions**

1106 674 The deposits of the Barberton Greenstone Belt host a large variety of convincing macro- and microscopic,  
1107 675 as well as geochemical evidence for early microbial life. It was predominantly thriving in shallow marine  
1108 676 environments in the photic zone but started to spread out to colonize fluvial habitats in emerged continental  
1109 677 surface environments and also occupied the first ecological niches, such as subsurface cavities. Traces of  
1110 678 ancient life in the BGB occur scattered throughout the entire stratigraphy confined to carbonaceous cherts  
1111 679 of the Onverwacht Group and siliciclastic deposits of the Moodies Group. However, their identification is  
1112 680 sometimes solely based on morphological attributes and not always accompanied by detailed and systematic

1116  
1117  
1118  
1119  
1120

1121  
1122  
1123 681 geochemical analysis at appropriate scales, which should be improved in future investigations. Due to their  
1124 682 wealth of remarkably preserved microbial mats and microfossils, consistent lateral exposure for several  
1125 683 tens of kilometers and thick stratigraphy, especially the deposits of the 3.416 Ga Buck Reef Chert and the  
1127 684 sandstones of the 3.22 Ga Moodies Group represent a unique window into a diverse Paleoproterozoic  
1128 685 biosphere.  
1130 686 Based on its universal and outstanding geological and paleobiological value the Barberton-Makhonjwa  
1131 687 Mountains were inscribed in the UNESCO World Heritage Site register in 2018, which will ultimately help  
1132 688 to protect these exceptional outcrops for future studies of Earth's early evolution.  
1134 689  
1135 690

1137 691 **Acknowledgements**

1138 692 This work was greatly supported by LabexMER ANR-10-LABX-19 and Prestige COFUND-GA-2013-  
1140 693 609102 to M.H. Amongst many others, the author would especially like to thank Maud Walsh, Gary Byerly,  
1141 694 Don Lowe, Christoph Heubeck, Dorothy Oehler, Wlady Altermann, and Andrew Knoll for their helpful  
1143 695 comments. I am also indebted to Stefan Lalonde and Claire Earlie for useful discussions and comments on  
1144 696 an earlier version of the manuscript.  
1146 697

1147 698

1148 699

1150 700 **References**

1151 701

1153 702 Ader, M., Thomazo, C., Sansjofre, P., Busigny, V., Papineau, D., Laffont, R., Cartigny, P., Halverson,  
1154 703 G.P., 2016. Interpretation of the nitrogen isotopic composition of Precambrian sedimentary rocks:  
1156 704 Assumptions and perspectives. *Chem. Geol.* 429, 93–110.  
1157 705 <https://doi.org/10.1016/j.chemgeo.2016.02.010>

1159 706 Alleon, J., Bernard, S., Le Guillou, C., Beyssac, O., Sugitani, K., Robert, F., 2018. Chemical nature of the  
1160 707 3.4 Ga Strelley Pool microfossils. *Geochemical Perspect. Lett.* 37–42.  
1162 708 <https://doi.org/10.7185/geochemlet.1817>

1163 709 Allwood, A.C., Rosing, M.T., Flannery, D.T., Hurowitz, J.A., Heirwegh, C.M., 2018. Reassessing  
1165 710 evidence of life in 3,700-million-year-old rocks of Greenland. *Nature*.  
1166 711 <https://doi.org/10.1038/s41586-018-0610-4>

1168 712 Allwood, A.C., Walter, M.R., Kamber, B.S., Marshall, C.P., Burch, I.W., 2006. Stromatolite reef from the  
1169 713 Early Archaean era of Australia. *Nature* 441, 714–718. <https://doi.org/10.1038/nature04764>

1171 714 Altermann, W., 2001. The oldest fossils of Africa – a brief reappraisal of reports from the Archean. *J.*

1172

1173

1174

1175

1176

1177  
1178  
1179 715 African Earth Sci. 33, 427–436. [https://doi.org/10.1016/S0899-5362\(01\)00089-6](https://doi.org/10.1016/S0899-5362(01)00089-6)  
1180 716 Anhaeusser, C.R., 1976. The geology of the sheba hills area of the Barberton Mountain Land, South  
1181 Africa with particular reference to the Eureka Syncline. *Trans. Geol. Soc. S. Africa* 79, 253–280.  
1182 717  
1183 718 Armstrong, R.A., Compston, W., de Wit, M., Williams, I.S., 1990. The stratigraphy of the 3.5–3.2 Ga  
1184 Barberton Greenstone Belt revisited: a single zircon ion microprobe study. *Earth Planet. Sci. Lett.*  
1185 719 101, 90–106.  
1186 720  
1187 721 Awramik, S.M., 1992. The oldest records of photosynthesis. *Photosynth. Res.* 33, 75–89.  
1188 722 <https://doi.org/10.1007/BF00039172>  
1189 723 Awramik, S.M., Buchheim, H.P., 2009. A giant, Late Archean lake system: The Meentheena Member  
1190 (Tumbiana Formation; Fortescue Group), Western Australia. *Precambrian Res.* 174, 215–240.  
1191 724 <https://doi.org/10.1016/j.precamres.2009.07.005>  
1192 725  
1193 726 Banerjee, N.R., Simonetti, A., Banerjee, N.R., Sciences, E., Ontario, W., Na, O., 2007. Direct dating of  
1194 Archean microbial ichnofossils Direct dating of Archean microbial ichnofossils.  
1195 727 <https://doi.org/10.1130/G23534A.1>  
1196 728  
1197 729 Barghoorn, E.S., 1971. The oldest fossils. *Sci. Am.* 224, 30–43.  
1200 730 Barghoorn, E.S., Schopf, J.W., 1966. Microorganisms Three Billion Years Old from the Precambrian of  
1201 South Africa. *Science (80-. )*. 152, 758–763. <https://doi.org/10.1126/science.152.3723.758>  
1202 731  
1203 732 Bosak, T., Bush, J.W.M., Flynn, M.R., Liang, B., Ono, S., Petroff, a. P., Sim, M.S., 2010. Formation and  
1204 stability of oxygen-rich bubbles that shape photosynthetic mats. *Geobiology* 8, 45–55.  
1205 733 <https://doi.org/10.1111/j.1472-4669.2009.00227.x>  
1206 734  
1207 735 Bose, S., Chafetz, H.S., 2009. Topographic control on distribution of modern microbially induced  
1208 sedimentary structures (MISS): A case study from Texas coast. *Sediment. Geol.* 213, 136–149.  
1209 736 <https://doi.org/10.1016/j.sedgeo.2008.11.009>  
1210 737  
1211 738 Brasier, M., McLoughlin, N., Green, O., Wacey, D., 2006. A fresh look at the fossil evidence for early  
1212 Archaeal cellular life. *Philos. Trans. R. Soc. Lond. B. Biol. Sci.* 361, 887–902.  
1213 739 <https://doi.org/10.1098/rstb.2006.1835>  
1214 740  
1215 741 Brooks, J., Muir, M.D., Shaw, G., 1973. Chemistry and Morphology of Precambrian Microorganisms.  
1216 742 *Nature* 244, 215–217. <https://doi.org/10.1038/244215a0>  
1217 743 Brooks, J., Shaw, G., 1971. Evidence for Life in the Oldest Known Sedimentary Rocks—the Onverwacht  
1218 Series Chert, Swaziland System of Southern Africa. *Grana* 11, 1–8.  
1219 744 <https://doi.org/10.1080/00173137109427403>  
1220 745  
1221 746 Buck, S.G., 1980. Stromatolite and ooid deposits within the fluvial and lacustrine sediments of the  
1222 Precambrian Ventersdorp Supergroup of South Africa. *Precambrian Res.* 12, 311–330.  
1223 747 [https://doi.org/10.1016/0301-9268\(80\)90033-9](https://doi.org/10.1016/0301-9268(80)90033-9)  
1224 748  
1225  
1226  
1227  
1228  
1229  
1230  
1231  
1232

1233  
1234  
1235 749 Buick, R., 2010. Early life: Ancient acritarchs. *Nature* 463, 885–886. <https://doi.org/10.1038/463885a>  
1236 750 Buick, R., 1992. The antiquity of oxygenic photosynthesis: evidence from stromatolites in sulphate-  
1237 deficient Archean lakes. *Science* (80-. ). 255, 74–77. <https://doi.org/10.1126/science.11536492>  
1238 751  
1239 752 Byerly, G.R., 1999. Komatiites of the Mendon Formation: Late-stage ultramafic volcanism in the  
1240 Barberton Greenstone Belt, in: Lowe, D.R., Byerly, G.R. (Eds.), *Geologic Evolution of the*  
1241 *Barberton Greenstone Belt, South Africa*. Geological Society of America, p. 0.  
1242 754  
1243 755 <https://doi.org/10.1130/0-8137-2329-9.189>  
1244  
1245 756 Byerly, G.R., Lowe, D.R., Heubeck, C., 2019. Geologic Evolution of the Barberton Greenstone Belt—A  
1246 Unique Record of Crustal Development, Surface Processes, and Early Life 3.55–3.20 Ga, in: *Earth’s*  
1247 *Oldest Rocks*. Elsevier, pp. 569–613. <https://doi.org/10.1016/B978-0-444-63901-1.00024-1>  
1248 758  
1249 759 Byerly, G.R., Lowe, D.R., Walsh, M.M., 1986. Stromatolites from the 3,300–3,500-Myr Swaziland  
1250 Supergroup, Barberton Mountain Land, South Africa. *Nature* 319, 489–491.  
1251 760  
1252 761 Byerly, G.R., Palmer, M.R., 1991. Tourmaline mineralization in the Barberton greenstone belt, South  
1253 Africa: early Archean metasomatism by evaporite-derived boron. *Contrib. to Mineral. Petrol.* 107,  
1254 762 387–402. <https://doi.org/10.1007/BF00325106>  
1255 763  
1256 764 Cardona, T., Sánchez-Baracaldo, P., Rutherford, A.W., Larkum, A.W., 2018. Early Archean origin of  
1257 Photosystem II. *Geobiology* 4, e00548. <https://doi.org/10.1111/gbi.12322>  
1258 765  
1259 766 Coffey, J.M., Flannery, D.T., Walter, M.R., George, S.C., 2013. Sedimentology, stratigraphy and  
1260 geochemistry of a stromatolite biofacies in the 2.72Ga Tumbiana Formation, Fortescue Group,  
1261 767 Western Australia. *Precambrian Res.* 236, 282–296.  
1262 768  
1263 769 <https://doi.org/10.1016/j.precamres.2013.07.021>  
1264  
1265 770 De Ronde, C.E.J., De Wit, M.J., 1994. Tectonic history of the Barberton greenstone belt, South Africa:  
1266 490 million years of Archean crustal evolution. *Tectonics* 13, 983–1005.  
1267 771  
1268 772 <https://doi.org/10.1029/94TC00353>  
1269  
1270 773 De Ronde, C.E.J., Kamo, S.L., 2000. An Archean arc-arc collisional event: A short-lived (ca 3 Myr)  
1271 774 episode, Weltevreden area, Barberton greenstone belt, South Africa. *J. African Earth Sci.* 30, 219–  
1272 248. [https://doi.org/10.1016/S0899-5362\(00\)00017-8](https://doi.org/10.1016/S0899-5362(00)00017-8)  
1273 775  
1274 776 De Wit, M.J., Furnes, H., R., 2011. Geology and tectonostratigraphy of the Onverwacht Suite, Barberton  
1275 Greenstone Belt. *Precambrian Res.* 186, 28–50.  
1276 777  
1277 778 de Wit, M.J., Hart, R., Martin, A., Abbott, P., 1982. Archean abiogenic and probable biogenic structures  
1278 associated with mineralized hydrothermal vent systems and regional metasomatism, with  
1279 779 implications for greenstone belt studies. *Econ. Geol.* 77, 1783–1802.  
1280 780  
1281 781 <https://doi.org/10.2113/gsecongeo.77.8.1783>  
1282  
1283 782 Engel, A.E.J., Nagy, B., Nagy, L.A., Engel, C.G., Kremp, G.O.W., Drew, C.M., 1968. Alga-Like Forms  
1284  
1285  
1286  
1287  
1288



1289  
1290  
1291 783 in Onverwacht Series, South Africa: Oldest Recognized Lifelike Forms on Earth. *Science* (80-. ).  
1292 784 161, 1005–1008. <https://doi.org/10.1126/science.161.3845.1005>  
1293  
1294 785 Eriksson, K.A., 1979. Marginal marine depositional processes from the Archaean Moodies Group,  
1295 786 Barberton Mountain Land; South Africa: Evidence and significance. *Precambrian Res.* 8, 153–182.  
1296  
1297 787 Eriksson, K.A., 1977. Tidal deposits from the Archaean Moodies Group, Barberton Mountain Land,  
1298 788 South Africa. *Sediment. Geol.* 18, 257–281.  
1299  
1300 789 Fliegel, D., Simonetti, A., Furnes, H., 2010. In-situ dating of the Earth ' s oldest trace fossil.  
1301 790 <https://doi.org/10.1016/j.epsl.2010.09.008>  
1302  
1303 791 Furnes, H., 2004. Early Life Recorded in Archean Pillow Lavas. *Science* (80-. ). 304, 578–581.  
1304 792 <https://doi.org/10.1126/science.1095858>  
1305  
1306 793 Furnes, H., Banerjee, N.R., Staudigel, H., Muehlenbachs, K., McLoughlin, N., Wit, M. De, Kranendonk,  
1307 794 M. Van, 2007. Comparing petrographic signatures of bioalteration in recent to Mesoarchean pillow  
1308 795 lavas : Tracing subsurface life in oceanic igneous rocks 158, 156–176.  
1309  
1310 796 <https://doi.org/10.1016/j.precamres.2007.04.012>  
1311  
1312 797 Gamper, A., Heubeck, C., Demske, D., Hoehse, M., 2012. Composition and Microfacies of Archean  
1313 798 Microbial Mats (Moodies Group, ca. 3.22 Ga, South Africa), in: Noffke, N., Chafetz, H.S. (Eds.),  
1314 799 Microbial Mats in Siliclastic Depositional Systems Through Time. *SEPM (Society for Sedimentary*  
1315  
1316 800 *Geology)*, Tulsa, pp. 65–74. <https://doi.org/10.2110/sepmsp.101.065>  
1317 801 Gerdes, G., 2007. Structures Left by Modern Microbial Mats in Their Host Sediments, in: Schieber, J.,  
1318 802 Bose, P.K., Eriksson, P., Banerjee, S., Sarkar, S., Altermann, W., Catuneanu, O. (Eds.), *Atlas of*  
1319 803 *Microbial Mat Features Preserved within the Siliciclastic Rock Record.* Elsevier, Amsterdam, pp. 5–  
1320 804 38. [https://doi.org/10.1016/S1574-1966\(07\)02001-9](https://doi.org/10.1016/S1574-1966(07)02001-9)  
1321  
1322 805 Gerdes, G., Klenke, T., Noffke, N., 2000. Microbial signatures in peritidal siliciclastic sediments: a  
1324 806 catalogue. *Sedimentology* 47, 279–308.  
1325  
1326 807 Glikson, M., Duck, L.J., Golding, S.D., Hofmann, A., Bolhar, R., Webb, R., Baiano, J.C.F., Sly, L.I.,  
1327 808 2008. Microbial remains in some earliest Earth rocks: Comparison with a potential modern  
1328  
1329 809 analogue. *Precambrian Res.* 164, 187–200. <https://doi.org/10.1016/j.precamres.2008.05.002>  
1330  
1331 810 Grosch, E.G., McLoughlin, N., 2014. Reassessing the biogenicity of Earth's oldest trace fossil with  
1332 811 implications for biosignatures in the search for early life. *Proc. Natl. Acad. Sci.* 111, 8380–8385.  
1333 812 <https://doi.org/10.1073/pnas.1402565111>  
1334  
1335 813 Hall, A.L., 1918. The geology of the Barberton gold mining district. *Geol. Surv. South Africa Mem.* 9,  
1336 814 347.  
1337  
1338 815 Heinrichs, T.K., Reimer, T., 1977. Geology and tectonostratigraphy of the Onverwacht Suite, Barberton  
1339 816 greenstone belt, South Africa. *Econ. Geol.* 72, 1426–1441.  
1340  
1341  
1342  
1343  
1344

1345  
1346  
1347 817 Heubeck, C., 2009. An early ecosystem of Archean tidal microbial mats (Moodies Group, South Africa,  
1348 818 ca. 3.2 Ga). *Geology* 37, 931–934. <https://doi.org/10.1130/G30101A.1>  
1349  
1350 819 Heubeck, C., Bläsing, S., Grund, M., Drabon, N., Homann, M., Nabhan, S., 2016. Geological constraints  
1351 820 on Archean (3.22 Ga) coastal-zone processes from the Dycedale Syncline, Barberton Greenstone  
1352 821 Belt. *South African J. Geol.* 119, 495–518. <https://doi.org/10.2113/gssajg.119.3.495>  
1353  
1354 822 Heubeck, C., Engelhardt, J., Byerly, G.R., Zeh, A., Sell, B., Luber, T., Lowe, D.R., 2013. Timing of  
1355 823 deposition and deformation of the Moodies Group (Barberton Greenstone Belt, South Africa): Very-  
1356 824 high-resolution of Archaean surface processes. *Precambrian Res.* 231, 236–262.  
1357 825 <https://doi.org/10.1016/j.precamres.2013.03.021>  
1358  
1359 826 Heubeck, C., Lowe, D.R., 1999. Sedimentary petrography and provenance of the Archean Moodies Grou,  
1360 827 Barberton Greenstone Belt, in: Lowe, D.R., Byerly, G.R. (Eds.), *Geologic Evolution of the*  
1361 828 *Barberton Greenstone Belt, South Africa. Geological Society of America Special Paper 329*, pp.  
1362 829 259–286.  
1363  
1364 830 Heubeck, C., Lowe, D.R., 1994a. Depositional and tectonic setting of the Archean Moodies Group,  
1365 831 Barberton greenstone belt, South Africa. *Precambrian Res.* 68, 257–290.  
1366  
1367 832 Heubeck, C., Lowe, D.R., 1994b. Late syndepositional deformation and detachment tectonics in the  
1368 833 Barberton Greenstone Belt, South Africa. *Tectonics* 13, 1514–1536.  
1369  
1370 834 Hickman-Lewis, K., Cavalazzi, B., Foucher, F., Westall, F., 2018. Most ancient evidence for life in the  
1371 835 Barberton greenstone belt: Microbial mats and biofabrics of the ~3.47 Ga Middle Marker horizon.  
1372 836 *Precambrian Res.* 312, 45–67. <https://doi.org/10.1016/j.precamres.2018.04.007>  
1373  
1374 837 Hickman-Lewis, K., Westall, F., Cavalazzi, B., 2019. Traces of Early Life From the Barberton  
1375 838 Greenstone Belt, South Africa, in: *Earth's Oldest Rocks. Elsevier B.V.*, pp. 1029–1058.  
1376 839 <https://doi.org/10.1016/B978-0-444-63901-1.00042-3>  
1377  
1378 840 Hofmann, A., 2005. The geochemistry of sedimentary rocks from the Fig Tree Group, Barberton  
1379 841 greenstone belt: Implications for tectonic, hydrothermal and surface processes during mid-Archaean  
1380 842 times. *Precambrian Res.* 143, 23–49. <https://doi.org/10.1016/j.precamres.2005.09.005>  
1381  
1382 843 Hofmann, A., Bolhar, R., 2007. Carbonaceous cherts in the Barberton greenstone belt and their  
1383 844 significance for the study of early life in the Archean record. *Astrobiology* 7, 355–388.  
1384 845 <https://doi.org/10.1089/ast.2005.0288>  
1385  
1386 846 Hofmann, A., Harris, C., 2008. Silica alteration zones in the Barberton greenstone belt : A window into  
1387 847 subsea floor processes 3.5 – 3.3 Ga ago. *Chem. Geol.* 257, 221–239.  
1388 848 <https://doi.org/10.1016/j.chemgeo.2008.09.015>  
1389  
1390 849 Homann, M., Heubeck, C., Airo, A., Tice, M.M., 2015. Morphological adaptations of 3.22 Ga-old tufted  
1391 850 microbial mats to Archean coastal habitats (Moodies Group, Barberton Greenstone Belt, South  
1392  
1393  
1394  
1395  
1396  
1397  
1398  
1399  
1400

1401  
1402  
1403 851 Africa). *Precambrian Res.* 266, 47–64. <https://doi.org/10.1016/j.precamres.2015.04.018>  
1404 852 Homann, M., Heubeck, C., Bontognali, T.R.R., Bouvier, A.S., Baumgartner, L.P., Airo, A., 2016.  
1405 853 Evidence for cavity-dwelling microbial life in 3.22 Ga tidal deposits. *Geology* 44, 51–54.  
1406 854 <https://doi.org/10.1130/G37272.1>  
1407 855 Homann, M., Sansjofre, P., Van Zuilen, M., Heubeck, C., Gong, J., Killingsworth, B., Foster, I.S., Airo,  
1408 856 A., Van Kranendonk, M.J., Ader, M., Lalonde, S. V, 2018. Microbial life and biogeochemical  
1409 857 cycling on land 3,220 million years ago. *Nat. Geosci.* 11, 665–671. [https://doi.org/10.1038/s41561-](https://doi.org/10.1038/s41561-018-0190-9)  
1410 858 018-0190-9  
1411 859 House, C.H., Oehler, D.Z., Sugitani, K., Mimura, K., 2013. Carbon isotopic analyses of ca. 3.0 Ga  
1412 860 microstructures imply planktonic autotrophs inhabited earth’s early oceans. *Geology* 41, 651–654.  
1413 861 <https://doi.org/10.1130/G34055.1>  
1414 862 Jahnert, R.J., Collins, L.B., 2013. Controls on microbial activity and tidal flat evolution in Shark Bay,  
1415 863 Western Australia. *Sedimentology* 60, 1071–1099. <https://doi.org/10.1111/sed.12023>  
1416 864 Jakubowicz, M., Berkowski, B., Belka, Z., 2014. Cryptic coral-crinoid “hanging gardens” from the  
1417 865 Middle Devonian of southern Morocco. *Geology* 42, 119–122. <https://doi.org/10.1130/G35217.1>  
1418 866 Javaux, E.J., Marshall, C.P., Bekker, A., 2010. Organic-walled microfossils in 3.2-billion-year-old  
1419 867 shallow-marine siliciclastic deposits. *Nature* 463, 934–8. <https://doi.org/10.1038/nature08793>  
1420 868 Karkhanis, S.N., 1977. Artifacts produced by chemical processing of samples for micropalaeontology and  
1421 869 organic geochemistry - a note of caution. *Precambrian Res.* 4, 229–236.  
1422 870 [https://doi.org/10.1016/0301-9268\(77\)90015-8](https://doi.org/10.1016/0301-9268(77)90015-8)  
1423 871 Knauth, L.P., Lowe, D.R., 2003. High Archean climatic temperature inferred from oxygen isotope  
1424 872 geochemistry of cherts in the 3.5 Ga Swaziland Supergroup, South Africa. *Bull. Geol. Soc. Am.*  
1425 873 115, 566–580. [https://doi.org/10.1130/0016-7606\(2003\)115<0566:HACTIF>2.0.CO;2](https://doi.org/10.1130/0016-7606(2003)115<0566:HACTIF>2.0.CO;2)  
1426 874 Knoll, A.H., Barghoorn, E.S., 1977. Archean Microfossils Showing Cell Division from the Swaziland  
1427 875 System of South Africa. *Science* (80-. ). 198, 396–398.  
1428 876 <https://doi.org/10.1126/science.198.4315.396>  
1429 877 Kobluk, D.R., James, N.P., 1979. Cavity-dwelling organisms in Lower Cambrian patch reefs from  
1430 878 southern Labrador. *Lethaia* 12, 193–218. <https://doi.org/10.1111/j.1502-3931.1979.tb00997.x>  
1431 879 Kozawa, T., Sugitani, K., Oehler, D.Z., House, C.H., Saito, I., Watanabe, T., Gotoh, T., 2018. Early  
1432 880 Archean planktonic mode of life: Implications from fluid dynamics of lenticular microfossils.  
1433 881 *Geobiology* 1–14. <https://doi.org/10.1111/gbi.12319>  
1434 882 Kremer, B., Kaźmierczak, J., 2017. Cellularly preserved microbial fossils from ~3.4 Ga deposits of South  
1435 883 Africa: A testimony of early appearance of oxygenic life? *Precambrian Res.* 295, 117–129.  
1436 884 <https://doi.org/10.1016/j.precamres.2017.04.023>  
1437  
1438  
1439  
1440  
1441  
1442  
1443  
1444  
1445  
1446  
1447  
1448  
1449  
1450  
1451  
1452  
1453  
1454  
1455  
1456

1457  
1458  
1459 885 Kröner, A., Byerly, G.R., Lowe, D.R., 1991. Chronology of early Archaean granite-greenstone evolution  
1460 886 in the Barberton Mountain Land , South Africa , based on precise dating by single zircon  
1461  
1462 887 evaporation. *Earth Planet. Sci. Lett.* 103, 41–54.  
1463 888 Kröner, A., Hegner, E., Wendt, J.I., Byerly, G.R., 1996. The oldest part of the Barberton granitoid-  
1464  
1465 889 greenstone terrain, South Africa: evidence for crust formation between 3.5 and 3.7 Ga. *Precambrian*  
1466 890 *Res.* 78, 105–124. [https://doi.org/10.1016/0301-9268\(95\)00072-0](https://doi.org/10.1016/0301-9268(95)00072-0)  
1467  
1468 891 Lamb, S., Paris, I., 1988. Post-onverwacht group stratigraphy in the SE part of the Archaean Barbeton  
1469 892 greenstone belt. *J. African Earth Sci. (and Middle East)* 7, 285–306. [https://doi.org/10.1016/0899-](https://doi.org/10.1016/0899-5362(88)90074-7)  
1470 893 [5362\(88\)90074-7](https://doi.org/10.1016/0899-5362(88)90074-7)  
1471  
1472 894 Lanier, W.P., Lowe, D.R., 1982. Sedimentology of the Middle Marker (3.4 Ga), Onverwacht Group,  
1473 895 Transvaal, South Africa. *Precambrian Res.* 18, 237–260. [https://doi.org/10.1016/0301-](https://doi.org/10.1016/0301-9268(82)90012-2)  
1474 896 [9268\(82\)90012-2](https://doi.org/10.1016/0301-9268(82)90012-2)  
1475  
1476 897 Lepot, K., Williford, K.H., Ushikubo, T., Sugitani, K., Mimura, K., Spicuzza, M.J., Valley, J.W., 2013.  
1477 898 Texture-specific isotopic compositions in 3 . 4 Gyr old organic matter support selective preservation  
1478 899 in cell-like structures. *Geochim. Cosmochim. Acta* 112, 66–86.  
1480 900 <https://doi.org/10.1016/j.gca.2013.03.004>  
1481  
1482 901 Lowe, D.R., 1999a. Geologic evolution of the Barberton Greenstone Belt and vicinity, in: Lowe, D.R.,  
1483 902 Byerly, G. (Ed.), *Special Paper 329: Geologic Evolution of the Barberton Greenstone Belt, South*  
1484 903 *Africa. Geological Society of America*, pp. 287–312. <https://doi.org/10.1130/0-8137-2329-9.287>  
1485  
1486 904 Lowe, D.R., 1999b. Petrology and sedimentology of cherts and related silicified sedimentary rocks in the  
1487 905 Swaziland Supergroup, in: Lowe, D.R., Byerly, G.R. (Eds.), *Geologic Evolution of the Barberton*  
1488 906 *Greenstone Belt, South Africa. Geological Society of America*, p. 0. [https://doi.org/10.1130/0-8137-](https://doi.org/10.1130/0-8137-2329-9.83)  
1489 907 [2329-9.83](https://doi.org/10.1130/0-8137-2329-9.83)  
1490  
1491 908 Lowe, D.R., 1999c. Shallow-water sedimentation of accretionary lapilli-bearing strata of the Msauli  
1492 909 Chert: Evidence of explosive hydromagmatic komatiitic volcanism, in: *Special Paper 329: Geologic*  
1493 910 *Evolution of the Barberton Greenstone Belt, South Africa. Geological Society of America*, pp. 213–  
1494 911 232. <https://doi.org/10.1130/0-8137-2329-9.213>  
1495  
1496 912 Lowe, D.R., 1994. Accretionary history of the Archean Barberton greenstone belt (3.55-3.22 Ga),  
1497 913 southern Africa. *Geology* 22, 1099–1102.  
1498  
1499 914 Lowe, D.R., Byerly, G.R., 2018. The terrestrial record of Late Heavy Bombardment. *New Astron. Rev.*  
1500 915 81, 39–61. <https://doi.org/10.1016/j.newar.2018.03.002>  
1501  
1502 916 Lowe, D.R., Byerly, G.R., 2015. Geologic record of partial ocean evaporation triggered by giant asteroid  
1503 917 impacts, 3.29-3.23 billion years ago. *Geology* 43, 535–538. <https://doi.org/10.1130/G36665.1>  
1504  
1505 918 Lowe, D.R., Byerly, G.R., 2007. Ironstone bodies of the Barberton greenstone belt, South Africa:  
1506  
1507  
1508  
1509  
1510  
1511  
1512

1513  
1514  
1515 919 Products of a Cenozoic hydrological system, not Archean hydrothermal vents! *GSA Bull.* 119, 65–  
1516 920 87. <https://doi.org/10.1130/b25997.1>  
1517  
1518 921 Lowe, D.R., Byerly, G.R., 1999. Stratigraphy of the west-central part of the Barberton Greenstone Belt,  
1519 922 South Africa, in: Lowe, D.R., Byerly, G.R. (Eds.), *Geologic Evolution of the Barberton Greenstone*  
1520 923 *Belt, South Africa. Geological Society of America Special Paper 329*, pp. 1–36.  
1522 924 Lowe, D.R., Byerly, G.R., 1986. Early Archean silicate spherules of probable impact origin, South Africa  
1523 925 and Western Australia. *Geology* 14, 83. [https://doi.org/10.1130/0091-](https://doi.org/10.1130/0091-7613(1986)14<83:EASSOP>2.0.CO;2)  
1525 926 [7613\(1986\)14<83:EASSOP>2.0.CO;2](https://doi.org/10.1130/0091-7613(1986)14<83:EASSOP>2.0.CO;2)  
1526 927 Lowe, D.R., Byerly, G.R., Asaro, F., Kyte, F.J., 1989. Geological and Geochemical Record of 3400-  
1527 928 Million-Year-Old Terrestrial Meteorite Impacts. *Science* (80-. ). 245, 959–962.  
1529 929 <https://doi.org/10.1126/science.245.4921.959>  
1530  
1531 930 Lowe, D.R., Byerly, G.R., Heubeck, C., 2012. Geologic Map of the west-central Barberton Greenstone  
1532 931 Belt, in: South Africa, Scale 1:25,000. Geological Society of America Map and Chart Series No.  
1533 932 103, Boulder. <https://doi.org/10.1130/2012.MCH103>  
1534 933 Lowe, D.R., Knauth, L.P., 1977. Sedimentology of the Onverwacht Group (3.4 Billion Years), Transvaal,  
1535 934 South Africa, and Its Bearing on the Characteristics and Evolution of the Early Earth. *J. Geol.* 85,  
1536 935 699–723. <https://doi.org/10.1086/628358>  
1537 936 Lowe, D.R., Worrell, G.F., 1999. Sedimentology, mineralogy, and implications of silicified evaporites in  
1538 937 the Kromberg Formation, Barberton Greenstone Belt, South Africa, in: *Special Paper 329: Geologic*  
1539 938 *Evolution of the Barberton Greenstone Belt, South Africa. Geological Society of America*, pp. 167–  
1540 939 188. <https://doi.org/10.1130/0-8137-2329-9.167>  
1541 940 Mcloughlin, N., Grosch, E.G., Kilburn, M.R., Wacey, D., 2012. Sulfur isotope evidence for a  
1542 941 Paleoproterozoic subseafloor biosphere, Barberton, South Africa 1031–1035.  
1543 942 <https://doi.org/10.1130/G33313.1>  
1544 943 Muir, M.D., Grant, P.R., 1976. Micropalaeontological evidence from the Onverwacht Group, South  
1545 944 Africa, in: Windley, B.. (Ed.), *The Early History of the Earth*. John Wiley & Sons, New York, pp.  
1546 945 595–608.  
1547 946 Muir, M.D., Hall, D.O., 1974. Diverse microfossils in Precambrian Onverwacht group rocks of South  
1548 947 Africa. *Nature* 252, 376–378. <https://doi.org/10.1038/252376a0>  
1549 948 Nabhan, S., Lubber, T., Scheffler, F., Heubeck, C., 2016a. Climatic and geochemical implications of  
1550 949 Archean pedogenic gypsum in the Moodies Group (~3.2 Ga), Barberton Greenstone Belt, South  
1551 950 Africa. *Precambrian Res.* 275, 119–134. <https://doi.org/10.1016/j.precamres.2016.01.011>  
1552 951 Nabhan, S., Wiedenbeck, M., Milke, R., Heubeck, C., 2016b. Biogenic overgrowth on detrital pyrite in  
1553 952 ca. 3.2 Ga Archean paleosols. *Geology* 44, 763–766. <https://doi.org/10.1130/G38090.1>  
1554  
1555  
1556  
1557  
1558  
1559  
1560  
1561  
1562  
1563  
1564  
1565  
1566  
1567  
1568

1569  
1570  
1571 953 Nagy, B., Nagy, L.A., 1969. Early Pre-Cambrian Onverwacht Microstructures : Possibly the Oldest  
1572 954 Fossils on Earth? *Nature* 223, 1226–1229. <https://doi.org/10.1038/2231226a0>  
1573  
1574 955 Noffke, N., Eriksson, K.A., Hazen, R.M., Simpson, E.L., 2006. A new window into Early Archean life:  
1575 956 Microbial mats in Earth’s oldest siliciclastic tidal deposits (3.2 Ga Moodies Group, South Africa).  
1576 957 *Geology* 34, 253. <https://doi.org/10.1130/G22246.1>  
1578 958 Nutman, A.P., Bennett, V.C., Friend, C.R.L., Van Kranendonk, M.J., Chivas, A.R., 2016. Rapid  
1579 959 emergence of life shown by discovery of 3,700-million-year-old microbial structures. *Nature* 537,  
1580 960 535–538. <https://doi.org/10.1038/nature19355>  
1581 961  
1582 962 Oehler, D.Z., Schopf, J.W., Kvenvolden, K.A., 1972. Carbon Isotopic Studies of Organic Matter in  
1583 963 Precambrian Rocks. *Science* (80-. ). 175, 1246–1248. <https://doi.org/10.1126/science.175.4027.1246>  
1584 964  
1585 965 Oehler, D.Z., Walsh, M.M., Sugitani, K., Liu, M.C., House, C.H., 2017. Large and robust lenticular  
1586 966 microorganisms on the young Earth. *Precambrian Res.* 296, 112–119.  
1587 967  
1588 968 <https://doi.org/10.1016/j.precamres.2017.04.031>  
1589 969  
1590 970 Oehler, D.Z., Walter, M.R., Sugitani, K., Allwood, A., Meibom, A., Mostefaoui, S., Selo, M., Thomen,  
1591 971 A., Gibson, E.K., 2009. NanoSIMS : Insights to biogenicity and syngeneity of Archaean  
1592 972 carbonaceous structures 173, 70–78. <https://doi.org/10.1016/j.precamres.2009.01.001>  
1593 973  
1594 974 Otálora, F., Mazurier, A., Garcia-Ruiz, J.M., Van Kranendonk, M.J., Kotopoulou, E., El Albani, A.,  
1595 975 Garrido, C.J., 2018. A crystallographic study of crystalline casts and pseudomorphs from the 3.5 Ga  
1596 976 dresser formation, Pilbara Craton (Australia). *J. Appl. Crystallogr.* 51, 1050–1058.  
1597 977  
1598 978 <https://doi.org/10.1107/S1600576718007343>  
1599 979  
1600 980 Pflug, H.D., 1967. Structured organic remains from the Fig Tree Series (Precambrian) of the Barberton  
1601 981 mountain land (South Africa). *Rev. Palaeobot. Palynol.* 5, 9–29. <https://doi.org/10.1016/0034->  
1602 982 [6667\(67\)90205-9](https://doi.org/10.1016/0034-6667(67)90205-9)  
1603 983  
1604 984 Pflug, H.D., 1966. Structured organic remains from the Fig Tree Series (Precambrian) of the Barberton  
1605 985 Mountain land (South Africa). *Econ. Geol. Res. Unit, Univ. Witwatersrand, Johannesburg, Inform.*  
1606 986 *Circ.* 28, 14.  
1607 987  
1608 988 Pflug, H.D., Meinel, W., Neumann, K.H., Meinel, M., 1969. Entwicklungstendenzen des frühen Lebens  
1609 989 auf der Erde. *Naturwissenschaften* 56, 10–14. <https://doi.org/10.1007/BF00599585>  
1610 990  
1611 991 Rasmussen, B., Blake, T.S., Fletcher, I.R., Kilburn, M.R., 2009. Evidence for microbial life in  
1612 992 synsedimentary cavities from 2.75 Ga terrestrial environments. *Geology* 37, 423–426.  
1613 993  
1614 994 <https://doi.org/10.1130/G25300A.1>  
1615 995  
1616 996 Schieber, J., Bose, P.K., Eriksson, P.G., 2007. Atlas of microbial mat features preserved within the  
1617 997 siliciclastic rock record. Elsevier, Amsterdam.  
1618 998  
1619 999 Schopf, J.W., 2004. Geochemical and submicron-scale morphologic analyses of individual Precambrian  
1620  
1621  
1622  
1623  
1624

1625  
1626  
1627 987 microorganisms. *Geochemical Soc. Spec. Publ.* 365–375.  
1628 988 Schopf, J.W., 1975. Precambrian Paleobiology: Problems and Perspectives. *Annu. Rev. Earth Planet. Sci.*  
1629 989 3, 213–249. <https://doi.org/10.1146/annurev.ea.03.050175.001241>  
1631 990 Schopf, J.W., Barghoorn, E.S., 1967. Alga-Like Fossils from the Early Precambrian of South Africa.  
1632 991 *Science* (80-. ). 156, 508–512. <https://doi.org/10.1126/science.156.3774.508>  
1634 992 Schopf, J.W., Walter, M.R., 1983. Archean microfossils: new evidence of ancient microbes, in: Schopf,  
1635 993 J.W. (Ed.), *Earth's Earliest Biosphere: Its Origin and Evolution*. Princeton University Press,  
1636 994 Princeton, pp. 214–239.  
1638 995 Simpson, E.L., Eriksson, K.A., Mueller, W.U., 2012. 3.2 Ga eolian deposits from the Moodies Group,  
1639 996 Barberton Greenstone Belt, South Africa: Implications for the origin of first-cycle quartz  
1641 997 sandstones. *Precambrian Res.* 214–215, 185–191. <https://doi.org/10.1016/j.precamres.2012.01.019>  
1643 998 Sleep, N.H., Zahnle, K.J., Kasting, J.F., Morowitz, H.J., 1989. Annihilation of ecosystems by large  
1644 999 asteroid impacts on the early Earth. *Nature* 342, 139–142. <https://doi.org/10.1038/342139a0>  
1646 1000 Staudigel, H., Furnes, H., Dewit, M., 2015. Paleoarchean trace fossils in altered volcanic glass 112.  
1647 1001 <https://doi.org/10.1073/pnas.1421052112>  
1648 1002 Stüeken, E.E., Kipp, M.A., Koehler, M.C., Buick, R., 2016. The evolution of Earth's biogeochemical  
1650 1003 nitrogen cycle. *Earth-Science Rev.* 160, 220–239. <https://doi.org/10.1016/j.earscirev.2016.07.007>  
1651 1004 Sugitani, K., Grey, K., Allwood, A., Nagaoka, T., Mimura, K., Minami, M., Marshall, C.P., Van  
1653 1005 Kranendonk, M.J., Walter, M.R., 2007. Diverse microstructures from Archaean chert from the  
1654 1006 Mount Goldsworthy-Mount Grant area, Pilbara Craton, Western Australia: Microfossils,  
1655 1007 dubiofossils, or pseudofossils? *Precambrian Res.* 158, 228–262.  
1657 1008 <https://doi.org/10.1016/j.precamres.2007.03.006>  
1659 1009 Sugitani, K., Lepot, K., Nagaoka, T., Mimura, K., Van Kranendonk, M., Oehler, D.Z., Walter, M.R.,  
1660 1010 2010. Biogenicity of Morphologically Diverse Carbonaceous Microstructures from the *ca.* 3400 Ma  
1661 1011 Strelley Pool Formation, in the Pilbara Craton, Western Australia. *Astrobiology* 10, 899–920.  
1663 1012 <https://doi.org/10.1089/ast.2010.0513>  
1664 1013 Sugitani, K., Mimura, K., Nagaoka, T., Lepot, K., Takeuchi, M., 2013. Microfossil assemblage from the  
1666 1014 3400Ma Strelley Pool Formation in the Pilbara Craton, Western Australia: Results from a new  
1667 1015 locality. *Precambrian Res.* 226, 59–74. <https://doi.org/10.1016/j.precamres.2012.11.005>  
1669 1016 Taj, R.J., Aref, M. a. M., Schreiber, B.C., 2014. The influence of microbial mats on the formation of sand  
1670 1017 volcanoes and mounds in the Red Sea coastal plain, south Jeddah, Saudi Arabia. *Sediment. Geol.*  
1672 1018 311, 60–74. <https://doi.org/10.1016/j.sedgeo.2014.06.006>  
1673 1019 Tice, M.M., 2009. Environmental Controls on Photosynthetic Microbial Mat Distribution and  
1674 1020 Morphogenesis on a 3.42Ga Clastic-Starved Platform. *Astrobiology* 9, 989–1000.  
1676  
1677  
1678  
1679  
1680

1681  
1682  
1683 1021 Tice, M.M., Bostick, B.C., Lowe, D.R., 2004. Thermal history of the 3.5-3.2 Ga Onverwacht and Fig  
1684 1022 Tree Groups, Barberton greenstone belt, South Africa, inferred by Raman microspectroscopy of  
1685 1023 carbonaceous material. *Geology* 32, 37–40. <https://doi.org/10.1130/G19915.1>  
1687 1024 Tice, M.M., Lowe, D.R., 2006a. The origin of carbonaceous matter in pre-3.0 Ga greenstone terrains: A  
1688 1025 review and new evidence from the 3.42 Ga Buck Reef Chert. *Earth-Science Rev.* 76, 259–300.  
1690 1026 <https://doi.org/10.1016/j.earscirev.2006.03.003>  
1691 1027 Tice, M.M., Lowe, D.R., 2006b. Hydrogen-based carbon fixation in the earliest known photosynthetic  
1692 1028 organisms. *Geology* 34, 37. <https://doi.org/10.1130/G22012.1>  
1694 1029 Tice, M.M., Lowe, D.R., 2004. Photosynthetic microbial mats in the 3, 416-Myr-old ocean. *Nature* 431,  
1695 1030 549–552. <https://doi.org/10.1038/nature02920.1>.  
1697 1031 Tice, M.M., Thornton, D.C.O., Pope, M.C., Olszewski, T.D., Gong, J., 2011. Archean Microbial Mat  
1698 1032 Communities. *Annu. Rev. Earth Planet. Sci.* 39, 297–319. [https://doi.org/10.1146/annurev-earth-](https://doi.org/10.1146/annurev-earth-040809-152356)  
1700 1033 [040809-152356](https://doi.org/10.1146/annurev-earth-040809-152356)  
1702 1034 Toulkeridis, T., Goldstein, S.L., Clauer, N., Kröner, A., Todt, W., Schidlowski, M., 1998. Sm-Nd, Rb-Sr  
1703 1035 and Pb-Pb dating of silicic carbonates from the early Archaean Barberton Greenstone Belt, South  
1704 1036 Africa: evidence for post-depositional isotopic resetting at low temperature. *Precambrian Res.* 92,  
1706 1037 129–144.  
1707 1038 Trower, E.J., Lowe, D.R., 2016. Sedimentology of the ~3.3Ga upper Mendon Formation, Barberton  
1709 1039 Greenstone Belt, South Africa. *Precambrian Res.* 281, 473–494.  
1710 1040 <https://doi.org/10.1016/j.precamres.2016.06.003>  
1712 1041 Van Kranendonk, M.J., Philippot, P., Lepot, K., Bodorkos, S., Pirajno, F., 2008. Geological setting of  
1713 1042 Earth's oldest fossils in the ca. 3.5 Ga Dresser Formation, Pilbara Craton, Western Australia.  
1714 1043 *Precambrian Res.* 167, 93–124. <https://doi.org/10.1016/j.precamres.2008.07.003>  
1716 1044 van Zuilen, M.A., Chaussidon, M., Rollion-Bard, C., Marty, B., 2007. Carbonaceous cherts of the  
1717 1045 Barberton Greenstone Belt, South Africa: Isotopic, chemical and structural characteristics of  
1719 1046 individual microstructures. *Geochim. Cosmochim. Acta* 71, 655–669.  
1720 1047 <https://doi.org/10.1016/j.gca.2006.09.029>  
1722 1048 Viljoen, M.J., Viljoen, R.P., 1969. An introduction to the geology of the Barberton granite-greenstone  
1723 1049 terrain. *Spec. Publ. Geol. Soc. S. Afr* 2, 9–28.  
1725 1050 Visser, D., 1956. The geology of the Barberton area. *Geol. Soc. S. Afr. Spec. Publ.* 15, 253.  
1726 1051 Wacey, D., 2012. Earliest evidence for life on Earth: An Australian perspective. *Aust. J. Earth Sci.* 59,  
1727 1052 153–166. <https://doi.org/10.1080/08120099.2011.592989>  
1729 1053 Wacey, D., 2009. Early Life on Earth. A Practical Guide, Topics in Geobiology, Vol. 31. Springer.  
1730 1054 Wacey, D., Fisk, M., Saunders, M., Eiloart, K., Kong, C., 2017. Critical testing of potential cellular  
1731 1732  
1733  
1734  
1735  
1736



1737  
1738  
1739 1055 structures within microtubes in 145 Ma volcanic glass from the Argo Abyssal Plain. *Chem. Geol.*  
1740 1056 466, 575–587. <https://doi.org/10.1016/j.chemgeo.2017.07.006>  
1741  
1742 1057 Wacey, D., Noffke, N., Saunders, M., Guagliardo, P., Pyle, D.M., 2018a. Volcanogenic Pseudo-Fossils  
1743 1058 from the ~3.48 Ga Dresser Formation, Pilbara, Western Australia. *Astrobiology* 18, ast.2017.1734.  
1744  
1745 1059 <https://doi.org/10.1089/ast.2017.1734>  
1746 1060 Wacey, D., Saunders, M., Kong, C., 2018b. Remarkably preserved tephra from the 3430 Ma Strelley Pool  
1747  
1748 1061 Formation, Western Australia: Implications for the interpretation of Precambrian microfossils. *Earth*  
1749 1062 *Planet. Sci. Lett.* 487, 33–43. <https://doi.org/10.1016/j.epsl.2018.01.021>  
1750  
1751 1063 Walsh, M.M., 2004. Evaluation of Early Archean Volcaniclastic and Volcanic Flow Rocks as Possible  
1752 1064 Sites for Carbonaceous Fossil Microbes. *Astrobiology* 4, 429–437.  
1753  
1754 1065 <https://doi.org/10.1089/ast.2004.4.429>  
1755 1066 Walsh, M.M., 1992. Microfossils and possible microfossils from the Early Archean Onverwacht Group,  
1756 1067 Barberton Mountain Land, South Africa. *Precambrian Res.* 54, 271–293.  
1757  
1758 1068 Walsh, M.M., Lowe, D.R., 1999. Modes of accumulation of carbonaceous matter in the Early Archean: a  
1759 1069 petrographic and geochemical study of the carbonaceous cherts of the Swaziland Supergroup, in:  
1760  
1761 1070 Lowe, D.R., Byerly, G.R. (Eds.), *Geologic Evolution of the Barberton Greenstone Belt, South*  
1762 1071 *Africa. Geological Society of America Special Paper* 329, pp. 115–132.  
1763  
1764 1072 Walsh, M.M., Lowe, D.R., 1985. Filamentous microfossils from the 3,500-Myr-old Onverwacht Group,  
1765 1073 Barberton Mountain Land, South Africa. *Nature* 314, 530–531.  
1766  
1767 1074 Walter, M.R., Buick, R., Dunlop, J.S.R., 1980. Stromatolites 3,400-3,500 Myr old from the North Pole  
1768 1075 area, Western Australia. *Nature*. <https://doi.org/10.1038/284443a0>  
1769  
1770 1076 Westall, F., Campbell, K.A., Bréhéret, J.G., Foucher, F., Gautret, P., Hubert, A., Sorieul, S., Grassineau,  
1771 1077 N., Guido, D.M., 2015. Archean (3.33 Ga) microbe-sediment systems were diverse and flourished in  
1772 1078 a hydrothermal context. *Geology* 43, 615–618. <https://doi.org/10.1130/G36646.1>  
1773  
1774 1079 Westall, F., Cavalazzi, B., Lemelle, L., Marrocchi, Y., Rouzaud, J.N., Simionovici, A., Salomé, M.,  
1775 1080 Mostefaoui, S., Andreazza, C., Foucher, F., Toporski, J., Jauss, A., Thiel, V., Southam, G.,  
1776  
1777 1081 MacLean, L., Wirick, S., Hofmann, A., Meibom, A., Robert, F., Défarge, C., 2011. Implications of  
1778 1082 in situ calcification for photosynthesis in a ~3.3Ga-old microbial biofilm from the Barberton  
1779  
1780 1083 greenstone belt, South Africa. *Earth Planet. Sci. Lett.* 310, 468–479.  
1781 1084 <https://doi.org/10.1016/j.epsl.2011.08.029>  
1782  
1783 1085 Westall, F., de Ronde, C.E., Southam, G., Grassineau, N., Colas, M., Cockell, C., Lammer, H., 2006.  
1784 1086 Implications of a 3.472-3.333 Gyr-old subaerial microbial mat from the Barberton greenstone belt,  
1785  
1786 1087 South Africa for the UV environmental conditions on the early Earth. *Philos. Trans. R. Soc. B Biol.*  
1787 1088 *Sci.* 361, 1857–1876. <https://doi.org/10.1098/rstb.2006.1896>  
1788  
1789  
1790  
1791  
1792

1793  
1794  
1795 1089 Westall, F., De Wit, M.J., Dann, J., Van der Gaast, S., De Ronde, C.E.J., Gerneke, D., 2001. Early  
1796 1090 archeon fossil bacteria and biofilms in hydrothermally-influenced sediments from the Barberton  
1797 greenstone belt, South Africa. *Precambrian Res.* 106, 93–116. <https://doi.org/10.1016/S0301->  
1798 1091 9268(00)00127-3  
1799 1092  
1800  
1801 1093 Westall, F., Hickman-Lewis, K., Hinman, N., Gautret, P., Campbell, K.A., Bréhéret, J.G., Foucher, F.,  
1802 1094 Hubert, A., Sorieul, S., Dass, A.V., Kee, T.P., Georgelin, T., Brack, A., 2018. A Hydrothermal-  
1803 1095 Sedimentary Context for the Origin of Life. *Astrobiology* 18, 259–293.  
1804 1096 <https://doi.org/10.1089/ast.2017.1680>  
1805 1097  
1806 1097 Williford, K.H., Ushikubo, T., Lepot, K., Kitajima, K., Hallmann, C., Spicuzza, M.J., Kozdon, R.,  
1807 1098 Eigenbrode, J.L., Summons, R.E., Valley, J.W., 2016. Carbon and sulfur isotopic signatures of  
1808 1099 ancient life and environment at the microbial scale: Neoproterozoic shales and carbonates. *Geobiology*  
1809 1100 14, 105–128. <https://doi.org/10.1111/gbi.12163>  
1810 1101  
1811 1101 Williford, K.H., Ushikubo, T., Schopf, J.W., Lepot, K., Kitajima, K., Valley, J.W., 2013. Preservation  
1812 1102 and detection of microstructural and taxonomic correlations in the carbon isotopic compositions of  
1813 1103 individual Precambrian microfossils. *Geochim. Cosmochim. Acta* 104, 165–182.  
1814 1104 <https://doi.org/10.1016/j.gca.2012.11.005>  
1815 1105  
1816 1105 Xie, X., Byerly, G.R., Ferrell Jr., R.E., 1997. IIB trioctahedral chlorite from the Barberton greenstone belt:  
1817 1106 crystal structure and rock composition constraints with implications to geothermometry. *Contrib. to*  
1818 1107 *Mineral. Petrol.* 126, 275–291. <https://doi.org/10.1007/s004100050250>  
1819 1108  
1820  
1821  
1822  
1823  
1824  
1825  
1826  
1827  
1828  
1829  
1830  
1831  
1832  
1833  
1834  
1835  
1836  
1837  
1838  
1839  
1840  
1841  
1842  
1843  
1844  
1845  
1846  
1847  
1848

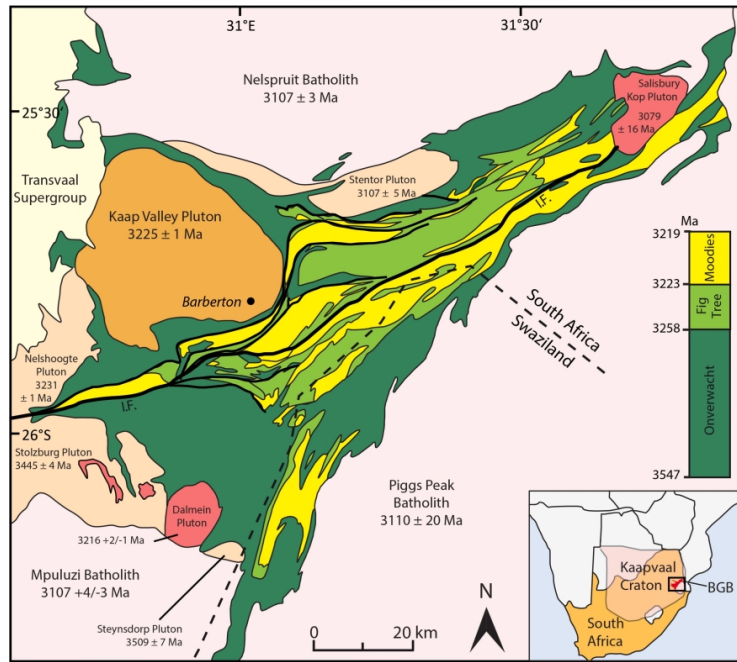


Fig. 1. Geological map of the Barberton Greenstone Belt (BGB) of South Africa and Swaziland and its surrounding plutons in the eastern part of the Kaapvaal Craton. The Barberton Supergroup comprises from base to top the Onverwacht, Fig Tree, and Moodies Group.

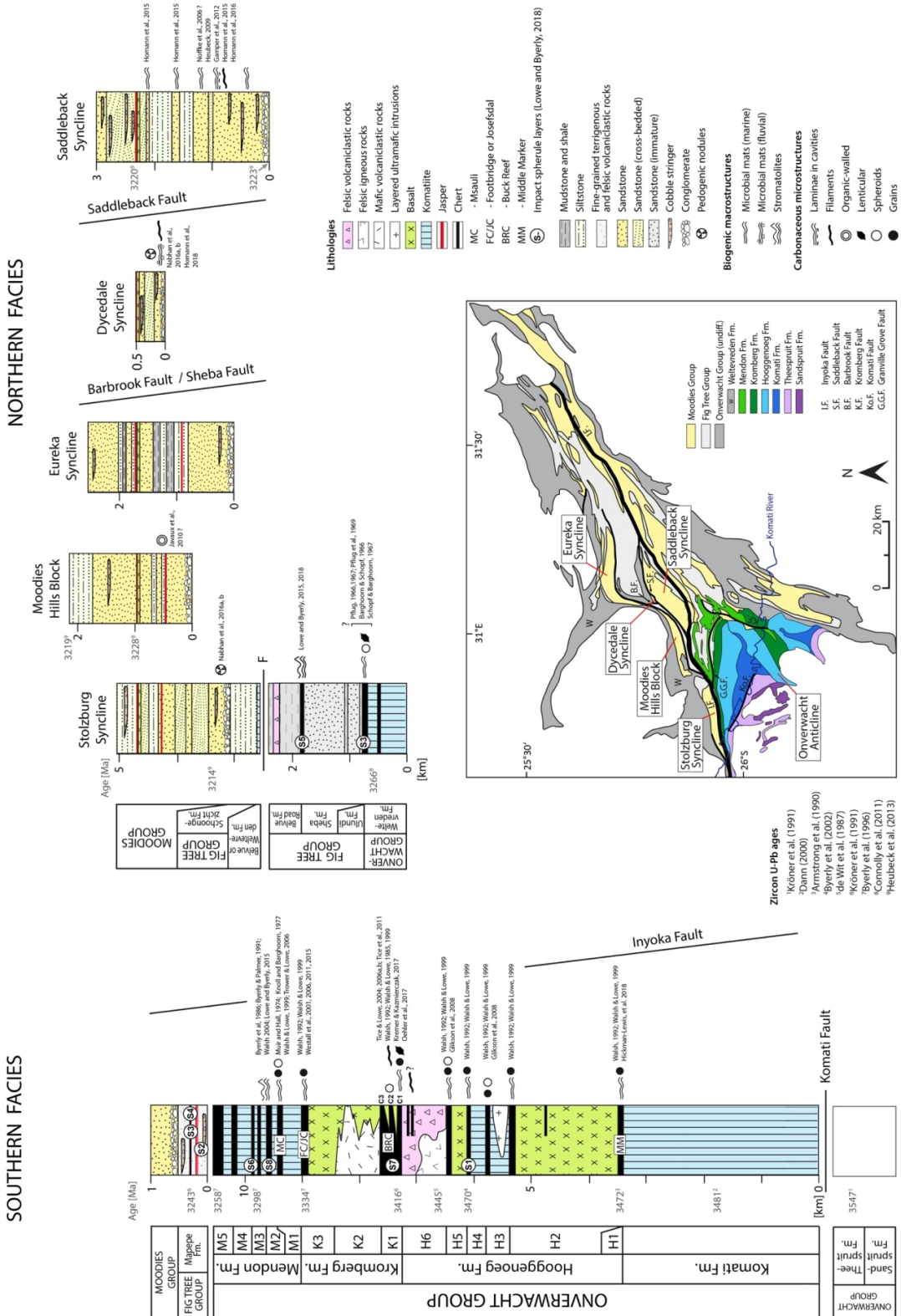


Fig. 2. Generalized stratigraphy and structure of the Barberton Supergroup north and south of the Inyoka Fault (mod. after Lowe and Byerly, 1999) with indicated stratigraphic position of reported macro- and microscopic traces of Paleoarchean life in the Barberton Greenstone Belt.

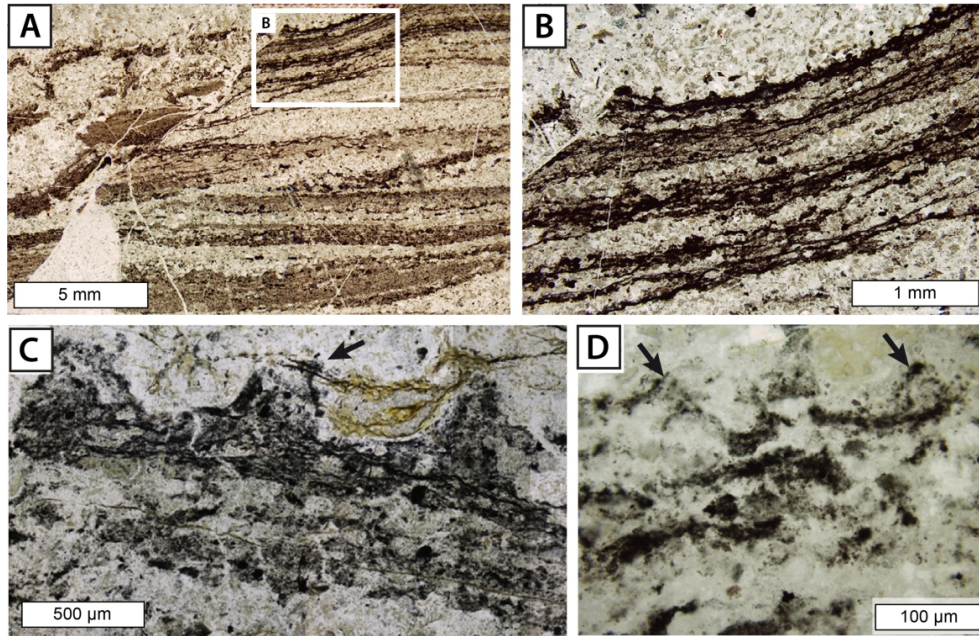


Fig. 3. Photomicrographs of carbonaceous laminations from silicified volcaniclastic sediments of the 3.47 Ga Middle Marker interpreted as remnants of microbial mats. A) Multi-layered mats on horizontally-laminated and cross-bedded sediments, disrupted by secondary fracture. B) Close-up view of crinkly, 'micro-tufted' laminations. C and D) Laminations with secondary 'pseudo-tufted' morphology (arrows), which likely formed due to plastic deformation. *Images (A-D) from Hickman-Lewis et al. (2018).*

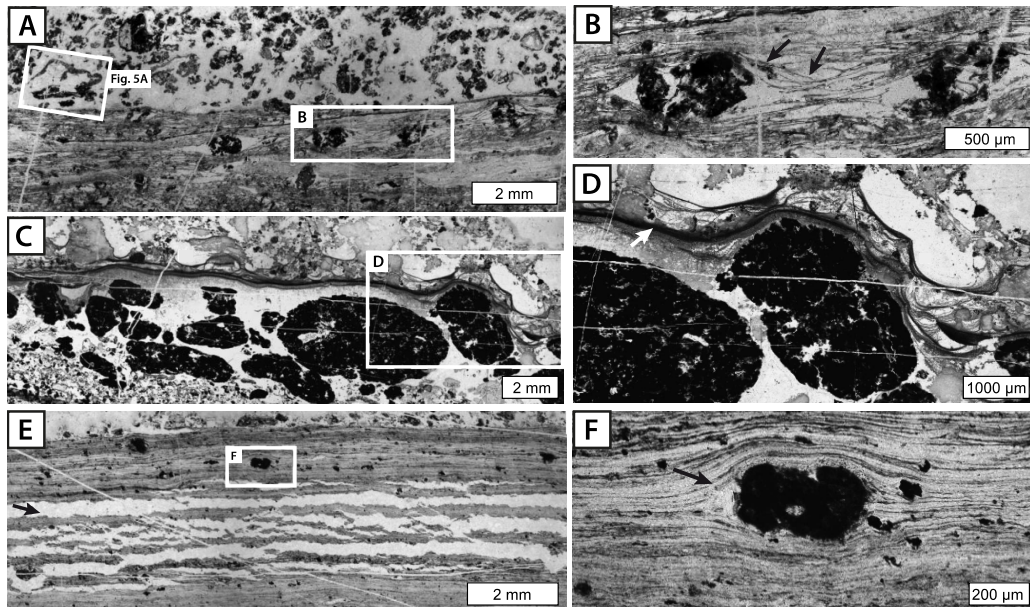


Fig. 4. Photomicrographs of morphologically diverse types of carbonaceous laminations preserved in the 3.42 Ga Buck Reef Chert and interpreted as fossil microbial mats. A and B) Alpha-type laminations loosely draping trapped grains (arrows) and overlain by detrital sediment layer with eroded mat fragment. C and D) Beta-type laminations with fine meshworks of filament-like strands that drape underlying detrital carbonaceous and silica grains (arrow). E) Gamma-type laminations dissected by early diagenetic silica veins subparallel to bedding (arrow), likely formed due to fluid escape from the sediment. F) Close-up view showing flat carbonaceous laminations, which tightly drape a detrital grain (arrow). *Images (A-F) from Tice (2009).*

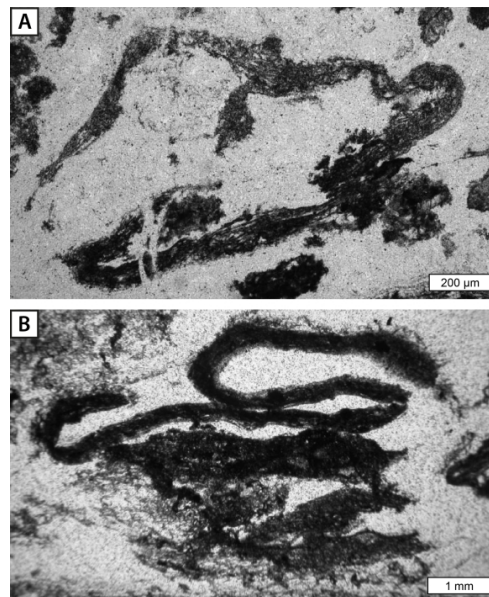


Fig. 5. Photomicrographs of eroded and rolled-up microbial mat fragments from the Buck Reef Chert. A) Close-up view of boxed area in Fig. 4A showing a plastically-deformed segment of alpha-type mat. B) Large, rolled-up fragment of a beta-type mat. *Image (A) from Tice (2009) and (B) from Tice and Lowe 2006b.*

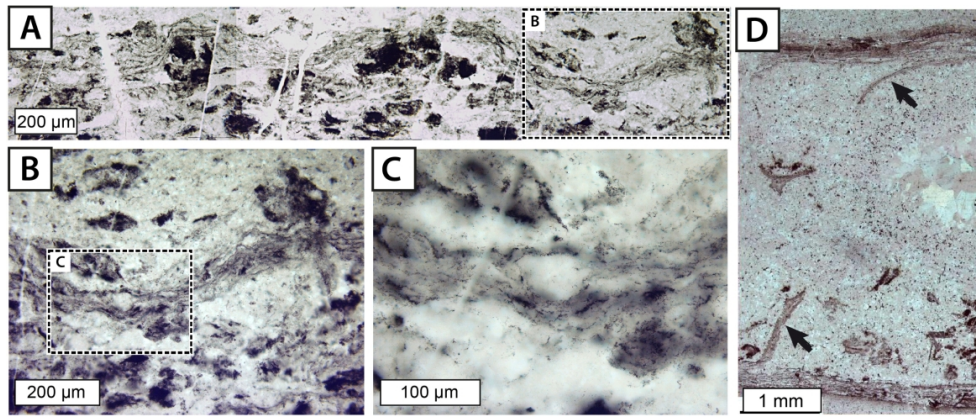


Fig. 6. Photomicrographs of microbial biofilms preserved in the 3.33 Ga Josefsdal Chert. A) Wispy anastomosing laminations that coat and stabilize the underlying sediments. B and C) Close-up views of the fine carbonaceous layers. D) Partially eroded fragments facing down and upwards (arrows) indicate pliable consistency of the biofilms. *Images (A-C) from Westall et al. (2011); Image (D) from Westall et al. (2015).*

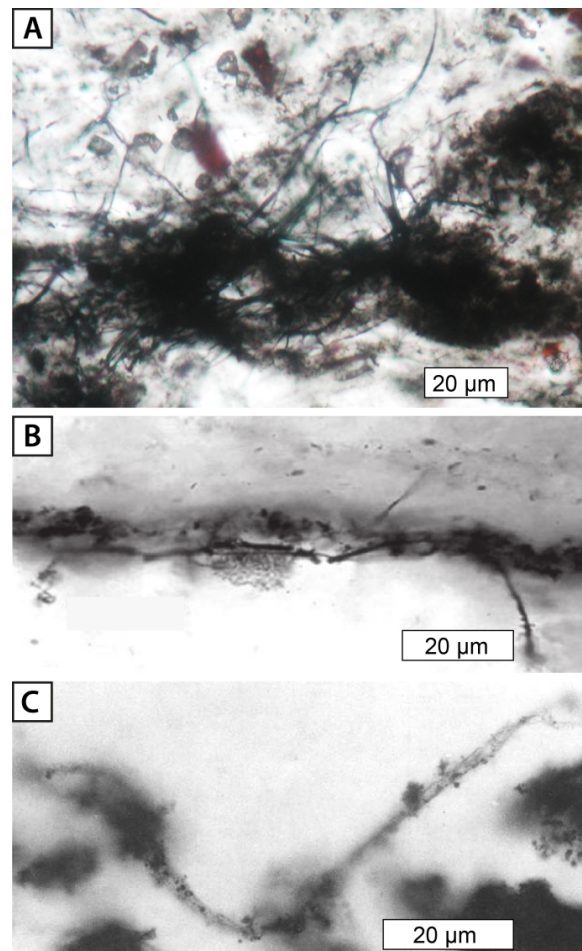


Fig. 7. Photomicrographs of filamentous microstructures from the Buck Reef Chert (Kromberg Formation). A) Interwoven clumps of filamentous microfossils. B) Hollow cylindrical filaments oriented subparallel to bedding. C) Solitary, slightly twisted hollow filament. *Image (A) courtesy of Maud M. Walsh; Image (B) from Walsh (2000); Image (C) from Walsh (1992).*

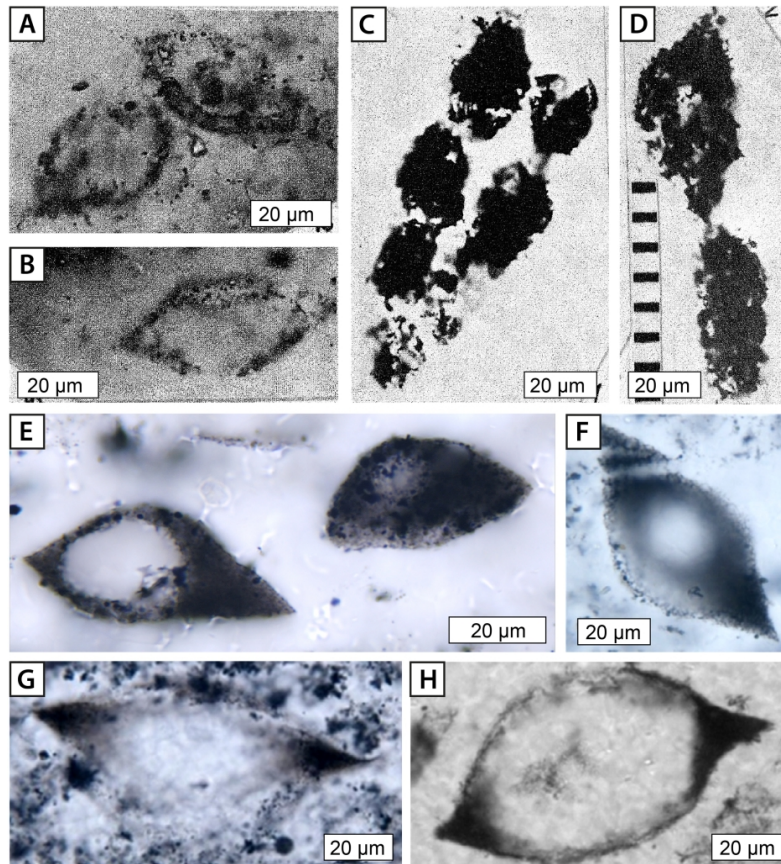


Fig. 8. Photomicrographs of lenticular structures interpreted as microfossils. A-D) Lenticular, disk-shaped objects with hollow centers and carbonaceous walls preserved in cherts from the Upper Onverwacht Group. Note that the structures occur isolated or in chain-like clusters of several specimen. (E-H) Morphologically very similar lenticular microfossils from the Buck Reef Chert. *Images (A-D) from Pflug (1966); Images (E-H) from Oehler et al. (2017), courtesy of Dorothy Z. Oehler.*



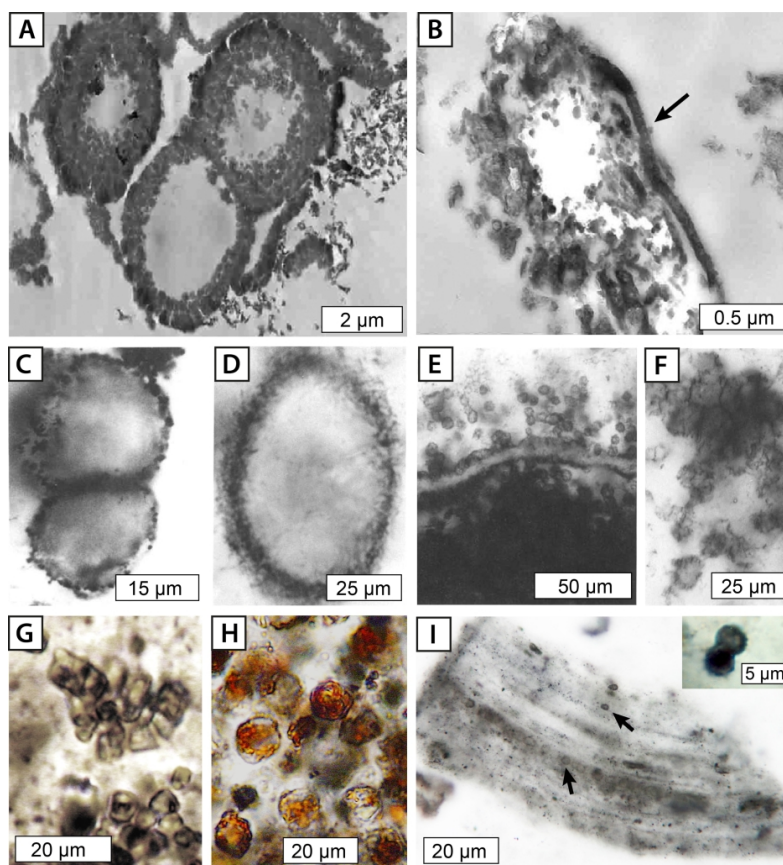
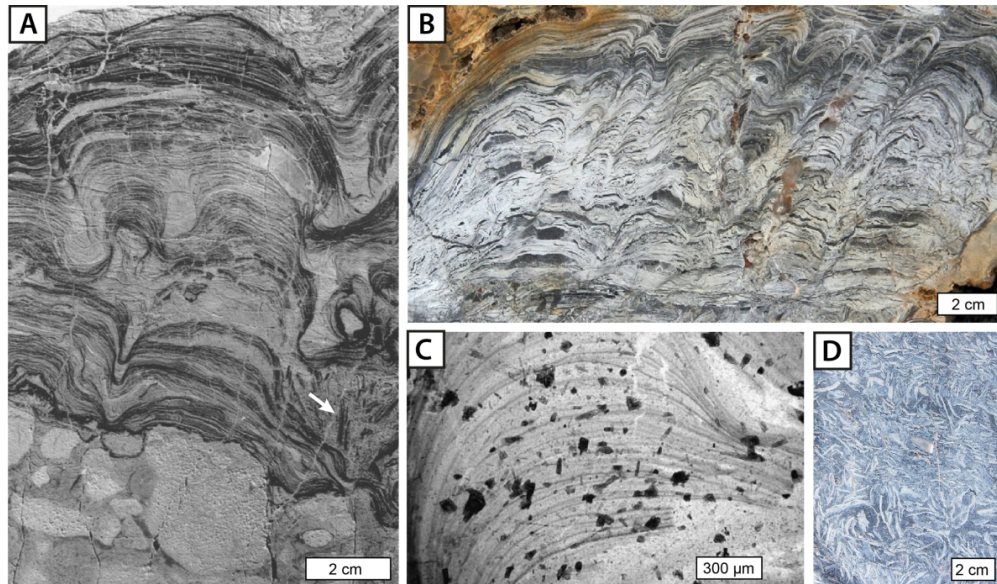


Fig. 9. Photomicrographs of proposed spheroidal microfossils from cherts of the Onverwacht Group. A and B) Transmission electron microscopy (TEM) images of cell-like objects with granular, in places detached walls (arrow) from the Hooggenoeg Formation. C and D) Large spheroids and ellipsoids from the Buck Reef Chert. E and F) Clusters of thin-walled spheroids from the Buck Reef Chert. G and H) Groups of spheroidal microstructures with rounded to angular walls from the Buck Reef Chert. I) Putative organic microspheres (arrows) from the Msauli Chert, which show features resembling cell division (small image in the upper right corner). Images (A-D) from Glikson *et al.* (2008); Images (C-F) from Walsh (1992); Images (G and H) from Kremer and Kazmierczak (2017); Image (I) courtesy of Andrew H. Knoll.



**Fig. 10.** Putative stromatolites and laminated silica crusts from the upper Onverwacht and Fig Tree Group. A) Polished slab showing morphologically diverse stromatolites overlying and draping the brecciated top of a komatiitic lava flow. Small basal domes successively grade into pseudocolumnar stromatolites with bridging laminations that are, in turn, overlain by low-relief domal laminations. Note the eroded stromatolite chips adjacent to the basal dome (arrow). B) Laminated silica crusts with inclined stromatolite-like columns and domes. C) Photomicrograph showing fine primary carbonaceous laminae with variable enrichment in secondary fine-grained tourmaline (dark minerals). D) Conglomerate of laminated silica chips interpreted as fragments of eroded stromatolites or sinter crusts. *Images (A and C) from Byerly and Palmer (1991), (B and D) from Lowe and Byerly (2018).*

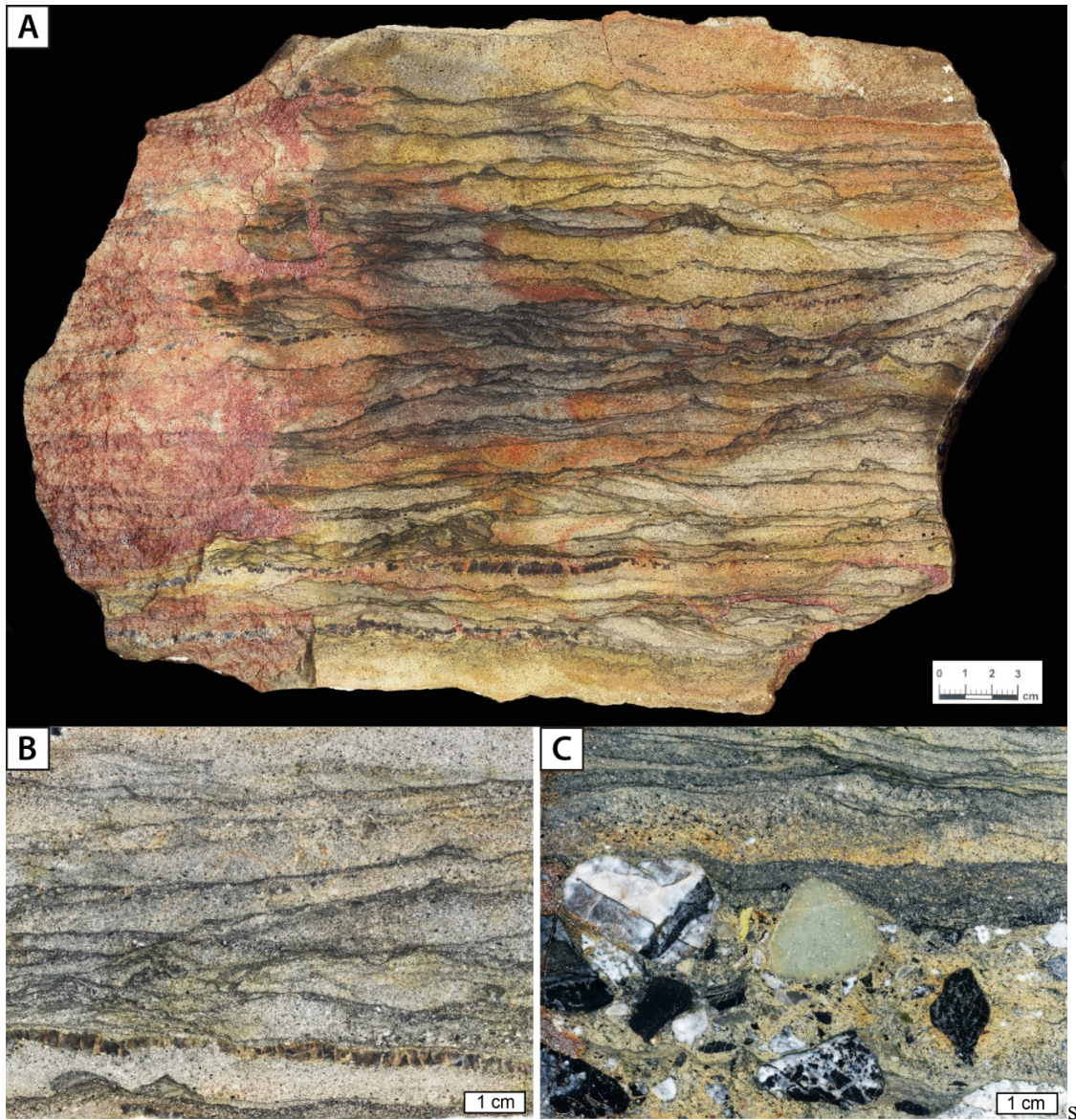


Fig. 11. Comparison of fossil microbial mats from tidal marine (A, B) and fluvial (C) deposits of the 3.22 Ga Moodies Group. A, B) Polished slab photographs of marine mats from the Saddleback Syncline showing densely spaced, crinkly carbonaceous laminations with small domes and tufts. The fossil mats are interbedded with medium- to coarse-grained sandstone and in places underlain by bedding-parallel chert lenses interpreted as silicified cavities. C) Terrestrial mats from the fluvial deposits of the Dycedale Syncline draping and onlapping interbedded clasts. Note that the preserved carbonaceous laminae are often thicker in comparison with the marine mats.

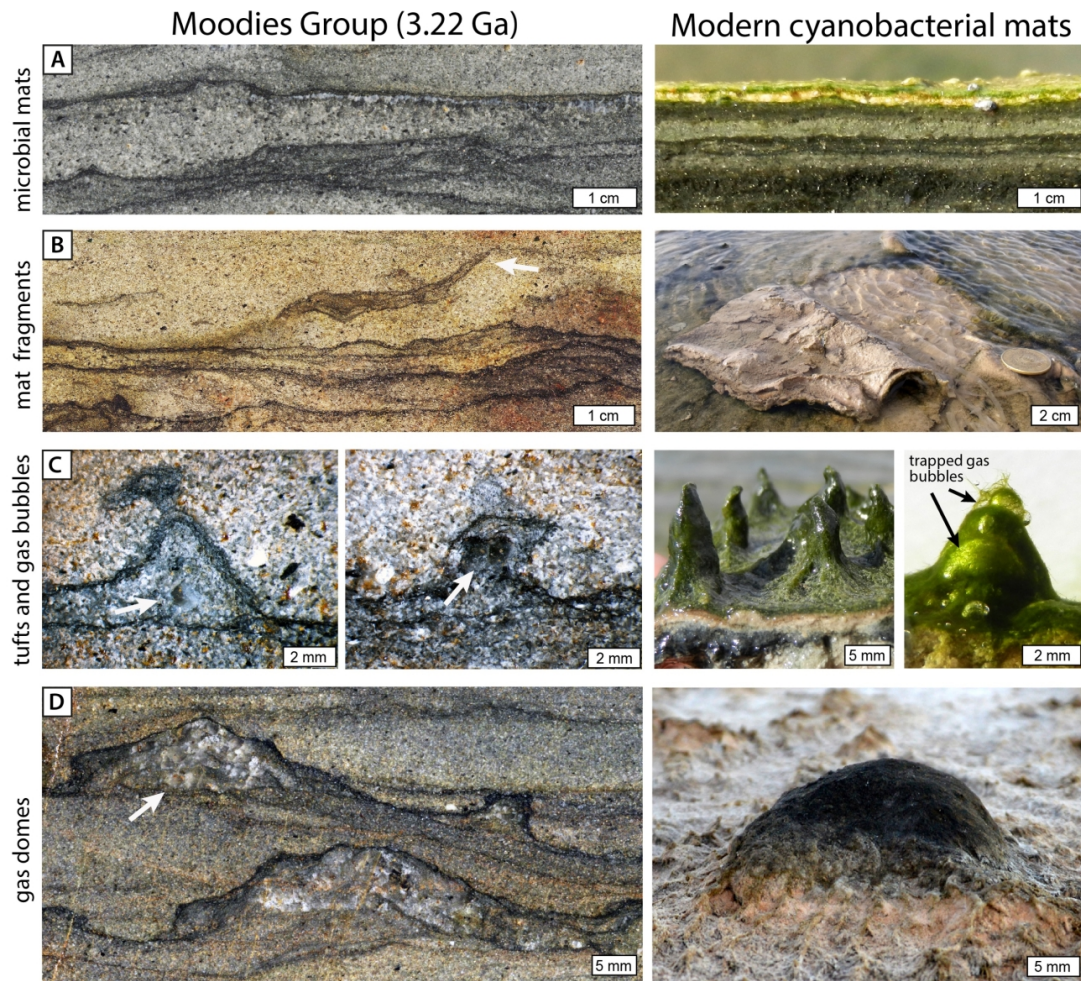


Fig. 12. Comparison of fossil intertidal microbial mats from the 3.22 Ga Moodies Group (left) with modern cyanobacterial mats from the tidal flats of Bahar Alouane, Tunisia (right). A) Crinkly carbonaceous mat laminations. B) Eroded mat fragment (arrow) and roll-up structure indicative for a cohesive consistency. C) Microbial tufts with now silicified cavities (arrows) interpreted as fossil gas bubbles, resembling trapped oxygen-rich bubbles in modern tufted mats. D) Silicified gas domes beneath the Moodies mats (arrow) and modern analogue of similar shape and size from Tunisia.

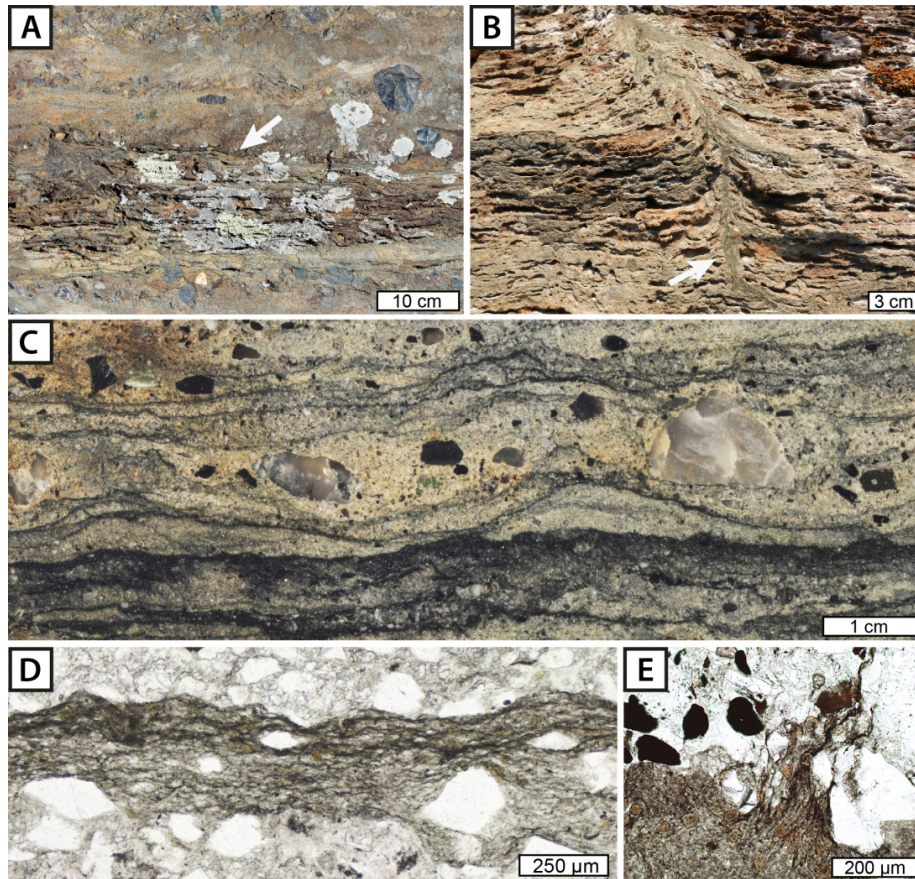


Fig. 13. Fossil terrestrial microbial mats from fluvial sandstones and conglomerates of the Moodies Group. A) Field photograph of the fluvial mats (arrow) interbedded with gravelly sandstones. B) Microbial mats disrupted and deformed by subvertical fluid-escape structure with well-defined central channel (arrow). C) Polished slab photograph with dark carbonaceous laminae of the fossil mats, draping former sedimentary surfaces and overlapping pebbles. D) Close-up view of the laminae, which show a dense meshwork of interwoven filamentous microstructures with trapped detrital grains. E) Filament-like microstructures in the upper, partially eroded part of the mat. *Images (A-E) from Homann et al. (2018).*

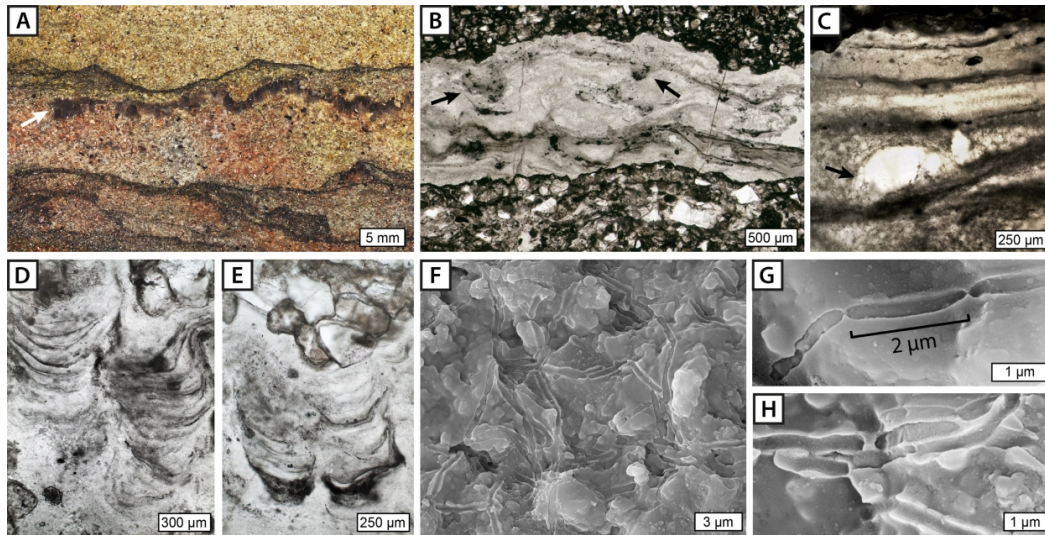


Fig. 14. Evidence for cavity-dwelling microbial life in the tidal deposits of the Moodies Group. A) Polished slab photograph showing silicified bedding-parallel cavity beneath fossil microbial mat (arrow). B) Photomicrograph of the silicified cavities with carbonaceous laminations, wisps, and pendant protrusions at the cavity ceiling (arrows). C) Carbonaceous laminae surrounding ovoid-shaped structure interpreted as trapped gas bubble (arrow). D and E) Close-up view of downward-facing columnar microstromatolites with preserved internal carbonaceous laminae. F) SEM image showing meshwork of filament molds embedded and permineralized in chert. G and H) Filamentous molds with regularly spaced, rod-shaped segments of approximately similar length. *Images (B and D-H) from Homann et al. (2016).*

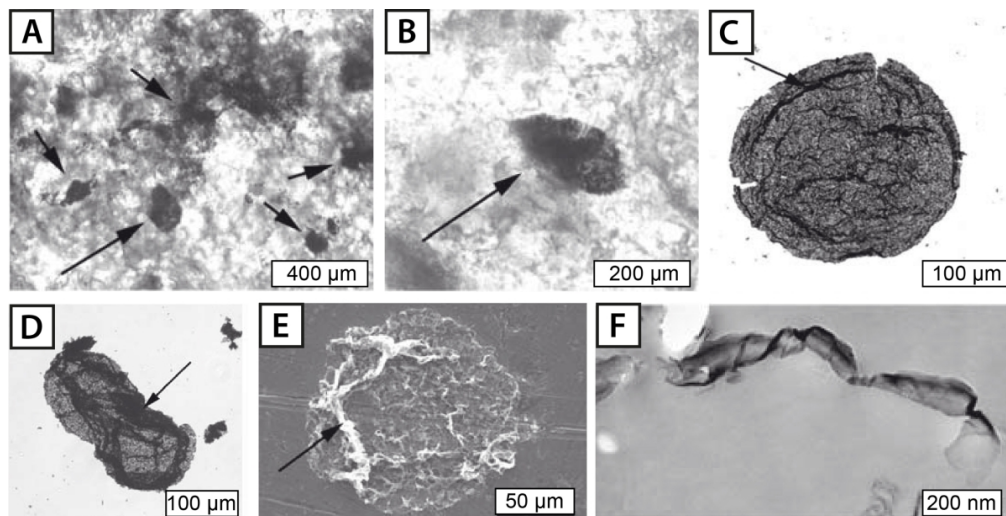


Fig. 15. Large organic-walled microfossils from the Moodies Group. A and B) Compressed spheroidal structures (arrows) in petrographic thin section. C and D) Microstructure extracted from the rock by acid maceration showing concentric folding (arrow in C) and collapse (arrow in D) of the wall. E) SEM image showing the folded, wrinkled and degraded texture of the wall (arrow). F) TEM image of ultrathin section showing homogenous ultrastructure of the torn and wrinkled 'cell' wall. *Images (A-F) from Javaux et al. (2010).*

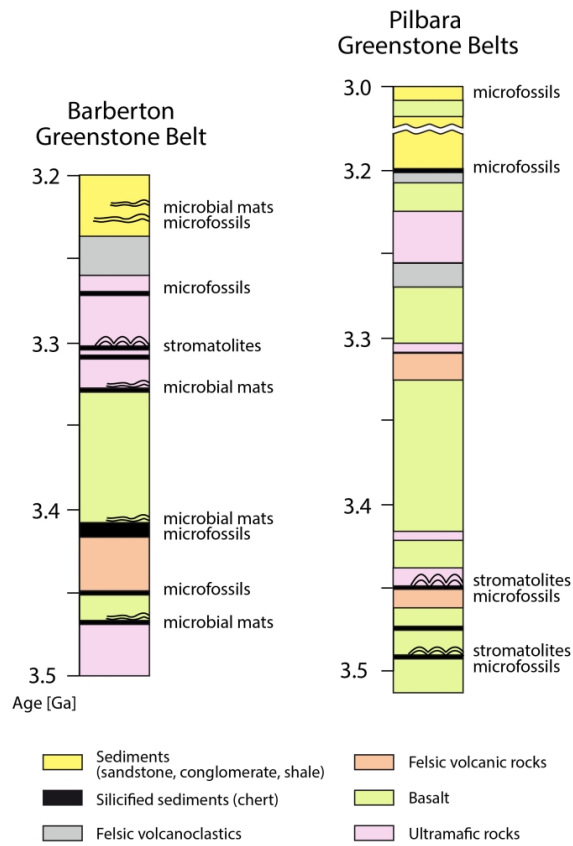


Fig. 15. Simplified stratigraphy and traces of early life in the Barberton Supergroup of South Africa in comparison with the Pilbara Supergroup of Western Australia.

**Table 1 | Claims for Paleoproterozoic Life in the Barberton Greenstone Belt, South Africa**

Age [Ma]	Lithostratigraphic Unit	Paleoenvironment	Morphological Evidence	Geochemical Evidence	Comments
~3220†	<b>Mooides Group</b>	Tidal marine coastline	<b>Microbial mats:</b> densely-spaced carbonaceous laminae interbedded with tidal sandstones (Nothke et al., 2006; Heubeck 2009; Gampert et al., 2012), cohesive erosion-resistant behavior, distinct mat morphologies (planar, crinkly, tufted); fossil gas bubbles, shrinkage cracks, eroded and reworked mat fragments, mm- to cm-sized silicified gas domes, and widespread fluid-escape structures (Homann et al., 2015).	$Bulk \delta^{13}C_{org}$ : -33.9‰ to -21.3‰ (n=30) $Bulk \delta^{15}N$ : -0.7‰ to +3.1‰ (n=9) Raman $T_{max}$ : ~366°C	Well-established depositional, and petrographic context, widespread occurrence (15 km along strike), facies depended mat morphology, combined with evidence for biogeochemical cycling of carbon and nitrogen strongly suggest a biogenic origin (Homann et al., 2018).
~3250	<b>Fig Tree Group</b> Sheba Fm.	Shallow-marine deltaic?	<b>Organic-walled microfossils:</b> of carbonaceous composition preserved in shales and siltstones, spheroidal shape (up to 300 µm in diameter), cellular morphology and ultrastructure, occurrence in populations (Javaux et al., 2010; Butck, 2010).	$Bulk \delta^{13}C_{org}$ : -28.3‰ to -16.4‰ (n=22)	A promising sign for life, carbon isotopes would be more convincing if measured in situ on individual microfossils.
		Braided fluvial to supratidal	<b>Paleosols:</b> containing pedogenic carbonates, sulfates, and pyrite grains with biogenic overgrowth rims (Nabhan et al., 2016a, b).	$In situ \delta^{34}S_{C-DTE}$ : -25‰ and -20‰ (n=105) suggestive for microbial fractionation of sulfur	Detailed stratigraphic and petrographic context support Earth's oldest known signs for biogenic sulfur cycling on land.
		Fluvial, coastal braidedplain	<b>Microbial mats:</b> of carbonaceous composition (Homann et al., 2018), draping gravely sandstone beds and conglomerates of fluvial-alluvial origin (Heubeck and Lowe, 1994; Eriksson et al., 2006; Heubeck et al., 2016) associated with desiccation cracks, eroded mat fragments and fluid-escape structures.	$Bulk \delta^{13}C_{org}$ : -23.6‰ to -17.9‰ (n=36) $Bulk \delta^{15}N$ : +1.9‰ to +5.6‰ (n=10) Raman $T_{max}$ : ~363°C	Earth's earliest combined fossil and geochemical evidence for the microbial colonization of terrestrial habitats on the emergent continental landmass.
3298±	<b>Onverwacht Group</b> Mendon Fm. (M2c)	Shallow-water to subaerial, evaporitic	<b>Stromatolites:</b> with tourmaline-rich, carbonaceous laminae preserved in cherts as laterally linked, low-relief domes (1–3 cm wide, 0.5–3 cm high) and compound domes or pseudocolumns of up to 10 cm height (Byerly et al., 1986; Byerly and Palmer, 1991). Fragments of eroded stromatolites or sinter crusts (Lowe and Byerly 2015, 2018).	None, except carbonaceous composition	Widespread (<10 km along strike) and morphological diverse. Possibly Africa's oldest stromatolites, but more evidence needed.
	Mendon Fm.* (previously named Swartkoppie Fm.)	?	<b>Possible microfossils:</b> lenticular [spindle-shaped] (30–70 µm in long axis) and spheroidal (5–50µm) shapes preserved in chert, occurrence as individuals or in clusters and chains, which might resemble remains of former colonies (Pflug 1966, 1967; Pflug et al., 1969). *Cherts were originally assigned to the Fig Tree Group.	None, except carbonaceous microfossil walls	Possible life, but geological context and geochemistry needed to further support biogenic origin.
	Mendon Fm.*	?	<b>Possible microfossils:</b> spheroidal structures, ~19 µm in diameter (Barghoorn and Schopf, 1966; Schopf and Barghoorn, 1967).	None, except carbonaceous microfossil walls	Simple morphology, and no depositional context or geochemistry reported. Could likely be non-biological (Wacey, 2009).
	Mendon Fm. (M1c) (Msauti Chert)	Shallow-marine to nearshore	<b>Possible microfossils:</b> spheroidal structures (1–4 µm in diameter) showing possible cell division (Knoll and Barghoorn, 1977).	None, except carbonaceous microfossil walls	Possible life, but hydrothermal fluids can mobilize and redistribute organic matter into spheroids (Knoll et al., 2016). High-resolution analysis needed to support biogenicity.



Age [Ma]	Lithostratigraphic Unit	Paleoenvironment	Morphological Evidence	Geochemical Evidence	Comments
3334 <sup>2</sup>	Kromberg Fm. (K3) (Loseisdal Chert)	Nearshore, possibly hydrothermal	<b>Microbial mats:</b> carbonaceous laminae (~10µm thick) in layered packets of 100–1000 µm thickness; eroded fragments of biofilms. (Westall et al., 2001; 2006; 2011; 2015). Putative rod-shaped microfossils are probably abiogenic (Altermann, 2001; Wacey 2009).	<i>Bulk</i> $\delta^{13}C_{org}$ : -26.8‰ and -22.7‰ (n=2) <i>In situ</i> : $\delta^{13}C_{org}$ : -45‰ to -13‰ $\delta^{34}S$ : -2.4‰	Petrographic observations and geochemical signals support the biogenic origin.
3416 <sup>3</sup>	Kromberg Fm. (K1) (Buck Reef Chert)	shallow-marine	<b>Microbial mats:</b> fine carbonaceous laminae with different morphotypes, draping underlying sediments and detrital particles; filaments (1–1.5 µm in diameter), rolled-up fragments; carbonaceous grains (Walsh and Lowe, 1999; Tice and Lowe, 2004a, 2006a, b; Tice, 2009; Tice et al., 2011). <b>Probable microfossils:</b> lenticular structures (1.3–1.35 µm long and 4.5–6.1 µm wide) with hollow center, interpreted as remnants of possibly planktonic microbes (Walsh, 1992; Oehler et al., 2017). Similar structures also occur in cherts of the Pilbara Craton. <b>Possible microfossils:</b> filamentous structures (1.2–1.4 µm in diameter), sometimes interwoven clumps spheroidal structures (1.0–8.4 µm and 4.5–12.8 µm in diameter) (Walsh and Lowe, 1985; Walsh 1992, 2000)	<i>Bulk</i> $\delta^{13}C_{org}$ : -36.9‰ and -20.1‰ (n=19) <i>In situ</i> $\delta^{13}C_{org}$ : -39.3‰ to -35.5‰ (n=8) None, except carbonaceous composition	Widespread, well-documented, and morphological complex evidence for life. Depositional context, morphological complexity, and narrow range of $\delta^{13}C_{org}$ values support a biological origin. High-resolution petrographic and <i>in situ</i> carbon isotope analysis needed.
3416 <sup>3</sup>	Kromberg Fm. (K1c2) (Buck Reef Chert)	shallow-marine	<b>Possible microfossils:</b> spheroidal (3–12 µm in diameter) interpreted as remains of beuthic-planktonic microbes, resembling coccolidal cyanobacteria (Krenner and Kazmierczak, 2017).	<i>Bulk</i> $\delta^{13}C_{org}$ : -26.5‰ and -24.3‰ (n=2)	Morphologically simple structures with angular terminations. Nanoscale analysis and <i>in situ</i> geochemical data needed.
~3450	Kromberg Fm. and Hoogenoeg Fm.	Submarine pillow basalts	<b>Possible trace fossils:</b> filament-shaped and titanite-mineralized microtubes (4 µm in diameter and up to 200µm in length) in glassy pillow lava rims (Furnes et al., 2004). Similarity to microtubes from recent pillow lavas, but even their microbial origin is debated (Wacey et al., 2017).	<i>Bulk</i> $\delta^{13}C_{carb}$ : -16.4‰ to +3.9‰ <i>In situ</i> $\delta^{34}S_{CDT}$ : -40‰ to -3‰ from pyrite	Syn- and biogenicity questioned by Grosch and McLaughlin (2014) and Grosch et al. (2016), structures likely formed abiotically during post depositional contact metamorphism.
	Hoogenoeg Fm.	?	<b>Possible microfossils:</b> spheroidal and cup-shaped structures; 5–106 µm in diameter (Engel et al., 1968).	None, except carbonaceous composition	Probably of non-biological origin (Nagy and Nagy, 1969; Schopf and Walter, 1983). Promising sign for life, but no geochemical data.
3470 <sup>4</sup>	Hoogenoeg Fm. (H3c, H5c)	Seafloor, possibly hydrothermal	<b>Possible microfossils:</b> spheroidal structures (2–10 µm in diameter) with granular 'cell' walls interpreted as remnants of chemosynthetic microbes (Glikson et al., 2008). Morphological similarity to modern hyperthermophilic microbes.	None	Promising sign for life, but no geochemical data.
3472 <sup>5</sup>	Hoogenoeg Fm. Middle Marker (H1)	Shallow marine, associated with volcanic activity	<b>Microbial mats:</b> fine, crinkly to micro-tufted laminations, 'trapped' detrital sediment, wisp-like microstructures interpreted as eroded biofilm or mat fragments (Hickman-Lewis et al., 2018).	None, except carbonaceous composition and REE data	Carbon isotope data needed to further support biogenicity of the possibly most ancient trace of life in the BCB.

**Age Dates:** <sup>1</sup>Heubbeck et al., 2013    <sup>2</sup>Byerly et al., 1999    <sup>3</sup>Kröner et al., 1991    <sup>4</sup>Byerly et al., 1999    <sup>5</sup>Armstrong et al., 1990